

**Effectiveness of emission control to reduce PM<sub>2.5</sub> pollution of Central China during winter haze episodes under various potential synoptic controls**

Yingying Yan <sup>1#</sup>, Yue Zhou <sup>2#</sup>, Shaofei Kong <sup>1,4\*</sup>, Jintai Lin <sup>3</sup>, Jian Wu <sup>1,4</sup>, Huang Zheng <sup>1,4</sup>, Zexuan Zhang <sup>1,4</sup>, Aili Song <sup>1</sup>, Yongqing Bai <sup>2</sup>, Zhang Ling <sup>2</sup>, Dantong Liu <sup>5</sup>, Tianliang Zhao <sup>6</sup>

<sup>1</sup> Department of Atmospheric Sciences, School of Environmental Studies, China University of Geosciences, Wuhan, 430074, China

<sup>2</sup> Hubei Key Laboratory for Heavy Rain Monitoring and Warning Research, Institute of Heavy Rain, China Meteorological Administration, Wuhan 430205, China

<sup>3</sup> Laboratory for Climate and Ocean-Atmosphere Studies, Department of Atmospheric and Oceanic Sciences, School of Physics, Peking University, Beijing 100871, China

<sup>4</sup> Department of Environmental Science and Engineering, School of Environmental Studies, China University of Geosciences, Wuhan, 430074, China

<sup>5</sup> Department of Atmospheric Sciences, School of Earth Sciences, Zhejiang University, Hangzhou, Zhejiang, China

<sup>6</sup> School of Atmospheric Physics, Nanjing University of Information Science and Technology, Nanjing, 210044, China

*Correspondence to: Shaofei Kong (kongshaofei@cug.edu.cn)*

<sup>#</sup> Contributed equally to this work

**Abstract**

Currently mitigating the severe particle pollution in autumn and winter is the key to further improve the air quality of China. The source contributions and transboundary transport of fine particles (PM<sub>2.5</sub>) in pollution episodes are closely related to large-scale or synoptic-scale atmospheric circulation. Under different synoptic conditions, how to effectively reduce emissions to control haze pollution is rarely reported. In this study, we classify the synoptic conditions over Central China from 2013 to 2018 by using

Lamb-Jenkenson method and the NCEP/NCAR FNL operational global analysis data. The effectiveness of emission control to reduce PM<sub>2.5</sub> pollution during winter haze episodes under potential synoptic controls is simulated by GEOS-Chem model. Among the ten identified synoptic patterns, four types account for 87% of the total pollution days. Two typical synoptic modes of them are characterized by small surface wind speed and stable weather conditions/high relative humidity (A/C-type) over Central China due to a high-pressure system/a southwest trough low-pressure system, blocking pollutants dispersion. Sensitivity simulations show that these two heavy pollution processes are mainly contributed by local emission sources with ~82% for A-type and ~85% for C-type, respectively. The other two patterns lead to pollution of transport characteristics affected by northerly/southerly winds (NW/SW-type), carrying air pollution from northern/southern China to Central China. The contribution of pollution transmission from North/South China is 36.9%/7.6% of PM<sub>2.5</sub> and local emission sources contribute 41%/69%. We also estimate the effectiveness of emission reduction in these four typical severe pollution synoptic processes. By only reducing SO<sub>2</sub> and NO<sub>x</sub> emission and not controlling NH<sub>3</sub>, the enhanced nitrate counteracts the effect of sulfate reduction on PM<sub>2.5</sub> mitigations, with less than 4% decrease in PM<sub>2.5</sub>. In addition, to effectively mitigate haze pollution of NW/SW-type synoptic controlled episodes, local emission control actions should be in coordination with regional collaborative actions.

## **1 Introduction**

The regional pollution of fine particles (PM<sub>2.5</sub>) has attracted worldwide attention in the public and in the scientific community (Cheng et al., 2016; Li et al., 2017c; Lin et al., 2018; Bi et al., 2019) due to its detrimental effect on visibility (Wang et al., 2020) and public health (Agarwal et al., 2017; Zhang et al., 2017). The PM<sub>2.5</sub> pollution in China has been continuously alleviating since 2013 as the implication of the Air Pollution Prevention and Control Action Plan (Zheng et al., 2018; Zhang et al., 2019),

especially in the Beijing-Tianjin-Hebei region (BTH) (Li et al., 2017b; Cheng et al., 2019), the Yangtze River Delta (YRD) region and the Pearl River Delta (PRD) region. However, severe particle pollution still occurs frequently in autumn and winter, which is the major reason restricting the  $PM_{2.5}$  to come up to national standard. For example, 12 extremely severe and persistent  $PM_{2.5}$  pollution episodes occurred in Beijing in January 2013, February 2014, December 2015, December 2016 and January 2017 (Zhong et al., 2018; Sun et al., 2016; Wang et al., 2018). Currently, how to effectively reduce emissions in autumn and winter is the key to mitigate haze pollution in China.

The contribution of emission sources has been widely recognized as the decisive factor of  $PM_{2.5}$  pollution over urban agglomerations, including industrial exhaust, urban transportation, residential emission, power plants, agricultural activities, and bio-combustion (Huang et al., 2014; Tian et al., 2016; Wu et al., 2018; An et al., 2019). While the outbreak, persistence and dissipation of particle pollution generally depends on the meteorological conditions and regional synoptic patterns, controlled by the large-scale or synoptic-scale atmospheric circulation (Chuang et al., 2008; Zhang et al., 2012; Russo et al., 2014; Zheng et al., 2015; Shu et al., 2017; Li et al., 2019).

Many studies have tried to reveal the relationship between synoptic patterns and severe particle pollution, and estimate the meteorological contributions to these pollution episodes. The YRD is mainly affected by pollutants transmitted from the northern and the southern China when the East Asian major trough is located at its front (Liao et al., 2017; Shu et al., 2017; Li et al., 2019). Liao et al. (2020) has confirmed that the relative position of the PRD to high-pressure systems imposes significant impacts on the diffusion conditions and the  $PM_{2.5}$  distributions in the PRD region. For North China Plain (NCP), high frequency of stagnant weather accompanied by small pressure gradient and near-surface wind speed, and shallow mixing layer are major reasons of aerosol pollution over this region in winter (He et al., 2018). The aerosol pollution formation process in Sichuan Basin is often controlled by the large scale high-pressure circulation at sea level (Sun et al., 2020). In the Guanzhong basin, pollution event is

generally governed by both the large-scale synoptic situation and the small-scale local circulation. The downhill wind not only forms a convergence zone in the basin, but also makes pollutants flow back from the mountain region to the basin (Bei et al., 2017). Leung et al. (2018) also find strong correlations of daily  $\text{PM}_{2.5}$  variability with several synoptic patterns, including monsoon flows and cold front channels in northern China related to the Siberian High, onshore flows in eastern China, and frontal rainstorms in southern China. These previous studies have highlighted that different levels of  $\text{PM}_{2.5}$  pollutions are closely related to the dominant synoptic patterns in different regions, and they attribute the large spatial variability of pollution to the regional transport contributions, not only the different local sources of  $\text{PM}_{2.5}$ . Thus, heavy pollution prevention and control needs to consider the weather situation, otherwise local emission reduction measures would not work well. However, under different synoptic conditions, how to effectively reduce local and regional emissions to control haze pollution is rarely reported.

Various key regions have issued the emergency preplan against the winter haze episodes, while these schemes can only be targeted at a certain city (The People's Government of Beijing Municipality, 2018; The People's Government of Shanghai Municipality, 2018) or a certain urban agglomeration (The People's Government of Guangdong Province, 2014). Although there are many studies targeted  $\text{PM}_{2.5}$  mitigations at a regional scale (Ding et al., 2019; Zhang et al., 2019, Xing et al., 2018, 2019; Fu et al., 2017; etc.), their results can not be directly applied to reduce winter  $\text{PM}_{2.5}$  pollution under various synoptic controls. Moreover, current emission reduction policies in China mainly aimed at sulfur dioxide ( $\text{SO}_2$ ) and nitrogen dioxide ( $\text{NO}_2$ ), ignoring the effective emission reduction on ammonia ( $\text{NH}_3$ ), although some modeling works have discussed the effectiveness of ammonia emission reduction for  $\text{PM}_{2.5}$  mitigations (Liu et al., 2019; Ye et al., 2019; Xu et al., 2019; Bai et al., 2019). Compared to remarkable reduction in  $\text{SO}_2$ ,  $\text{NO}_2$ , and primary PM emissions,  $\text{NH}_3$  emissions has remained stable during 2014–2018 in China (Zheng et al., 2018). In addition, given the

important roles of other  $\text{PM}_{2.5}$  precursors (eg., NMVOCs) in aerosol formation (Geng et al., 2019), cutting non- $\text{SO}_2$ - $\text{NO}_2$ -PM emissions should be proposed as a next-step mitigation strategy. Therefore, for  $\text{PM}_{2.5}$  mitigations in a specific region during winter haze episodes forced by various synoptic conditions, whether the air pollution emergency management and control schemes are effective and how to improve them have become an urgent scientific question to be answered.

In order to investigate the effectiveness of emission control to reduce  $\text{PM}_{2.5}$  pollution during winter haze episodes under various potential synoptic controls (PSCs), we take the severe particle pollution of winter haze episodes over Jingzhou, the hinterland of Yangtze River middle basin in Central China, as an example. Central China is geographically surrounded by major haze pollution regions, the SCB to the west, the PRD to the south, the YRD to the east, and the NCP to the north (Fig. 1). As a regional pollutant transport hub with sub basin topography, Central China is a region of transmission-pollution characteristics affected by two reported transport pathways from the vast flatland in central eastern China (Yu et al., 2020) and from the NCP region (Zheng et al., 2019a). In combination with high anthropogenic emissions (Wu et al., 2018) and secondary aerosol formation (Huang et al., 2020), Central China often suffers severe pollution episodes in winter caused by  $\text{PM}_{2.5}$  (Gong et al., 2015; Xu et al., 2017). In this study, we conduct the circulation classification to differentiate the synoptic modes during the severe particle pollution episodes in winter over Central China from 2013 to 2018 by using Lamb-Jenkenson method. Then we simulate the  $\text{PM}_{2.5}$  chemical components, and the contributions of local sources as well as transboundary transport of  $\text{PM}_{2.5}$  under different synoptic conditions. Finally, the effectiveness of emission reduction in main potential synoptic patterns are evaluated by GEOS-Chem model simulations. This study combines the atmospheric (circulation classification) and environmental (chemical transport modeling) research methods and could provide reference for emission control of severe winter haze pollution under different weather types, and provide basis for regional air quality policy-making.

## 2 Data and Methods

### 2.1 Data

Hourly mass concentrations of PM<sub>2.5</sub> at Jingzhou (112.18°E, 30.33°N, 33.7 m) from November 2013 to December 2018 are obtained from Hubei Environmental Monitoring Central Station (<http://sthjt.hubei.gov.cn/>). We screen the pollution days with daily mean PM<sub>2.5</sub> concentrations larger than 150 µg/m<sup>3</sup> for circulation classification.

Figure 1

We use the daily mean sea level pressure (SLP) between 2013 and 2018 from the National Centers for Environmental Prediction/National Center for Atmospheric Research (NCEP/NCAR) Final (FNL) Operational Global Analysis data (horizontal resolution: 1° × 1°; temporal resolution: 6 hours; <https://rda.ucar.edu/datasets/ds083.3/>) to conduct the classification of Lamb-Jenkenson circulation types.

The meteorological data of surface observations at Jingzhou, including ambient temperature, relative humidity, wind speed, wind direction and atmospheric pressure, are obtained from Hubei Meteorological Information and Technology Support Center (<http://hb.cma.gov.cn/qxfw/index.html>). The data from November 2013 to February 2014 are used to analyze the meteorological characteristics during the period four severe particle pollution events occurred in succession over Central China (Fig. S1).

In order to better evaluate the GEOS-Chem model performances, we also use the PM<sub>2.5</sub> observations (a total of 633 sites; from November 2013 to February 2014) from Ministry of Ecology and Environment of China (MEE, <http://www.mee.gov.cn/>) to conduct the model-observation comparison.

### 2.2 Lamb-Jenkenson Circulation Classification

The atmospheric circulation classification adopts the Lamb-Jenkenson method proposed by Lamb et al. (1950) and developed by Jenkenson et al. (1977). Compared to the objective classification method PCA used in some studies (Chang and Zhan, 2017, Dai et al., 2021), this Lamb-Jenkenson method is a combination of subjective and objective methods. After the objective judgment of the circulation, we also make subjective considerations to overcome the weaknesses of their respective, leading to better synoptic significance. Many works of circulation classification have used the Lamb-Jenkenson method and reported that the analysis can well respond to the classification results (Philipp et al., 2016; Santurtun et al., 2015; Pope et al., 2015; Russo et al., 2014; Pope et al., 2014; Trigo and DaCamara, 2000).

To calculate the circulation types of Jingzhou, we mark total 16 points (97.5°E-127.5°E, 20°N-40°N) by every 10 longitudes and 5 latitudes and the center point located at 112.5° E and 30° N (Fig. S2). Using the sea level pressure of 16 points, we calculate six circulation indexes by scheme of central difference:

$$u = 0.5[P(12) + P(13) - P(4) - P(5)] \quad (1)$$

$$v = \frac{1}{\cos \alpha} \times \frac{1}{4} [P(4) + 2P(9) + P(13) - P(4) - 2P(8) - P(12)] \quad (2)$$

$$V = \sqrt{u^2 + v^2} \quad (3)$$

$$\xi_u = \frac{\sin \alpha}{2 \sin \alpha_1} [P(15) + P(16) - P(8) - P(9)] - \frac{\sin \alpha}{2 \sin \alpha_2} [P(8) + P(9) - P(1) - P(2)] \quad (4)$$

$$\xi_v = \frac{1}{8 \cos^2 \alpha} [P(6) + 2P(10) + P(14) - P(5) - 2P(9) - P(13) + P(3) + 2P(7) + P(11) - P(4) - 2P(8) - P(12)] \quad (5)$$

194  $\xi = \xi_u + \xi_v$

195 (6)

196 Where  $P(n)(n=1,2,3\cdots 16)$  is the sea level pressure at the  $n^{\text{th}}$  point;  
 197  $\alpha, \alpha_1$  and  $\alpha_2$  are the latitude values of points  $C, A_1$  and  $A_2$ , respectively;  $v$  is the  
 198 geostrophic wind,  $u$  and  $v$  are the latitudinal and meridional components of the  
 199 geostrophic wind;  $\xi$  is the geostrophic vorticity;  $\xi_u$  is the  $u$  meridional gradient,  
 200 and  $\xi_v$  is the  $v$  latitudinal gradient.

201 Taking the latitude of the center point as the reference frame, the unit of six  
 202 circulation indexes is  $hPa/(10^\circ lon)$ , the direction of geostrophic wind can be  
 203 determined by  $u$  and  $v$ , and cyclones and anticyclones can be determined by  $\xi$ .  
 204 According to the geostrophic wind speed, wind direction and vorticity value, the  
 205 circulation is divided into 10 types. The classification standard and corresponding types  
 206 are shown in Table 1.

207

208 Table 1

209

### 210 2.3 GEOS-Chem simulations

211 The GEOS-Chem chemistry transport model is used  
 212 (<http://acmg.seas.harvard.edu/geos/>) to simulate the spatiotemporal distribution of  
 213  $PM_{2.5}$ . The nested model, covering China ( $70^\circ E-140^\circ E$ ,  $15^\circ S-55^\circ N$ ), is run with a  
 214 horizontal resolution of  $0.25^\circ$  latitude  $\times$   $0.3125^\circ$  longitude and 72 vertical layers. The  
 215 boundary condition of nested model is provided by the GEOS-Chem global model with  
 216 a horizontal resolution of  $2^\circ$  latitude  $\times$   $2.5^\circ$  longitude (Fig. S3). Both global and nested  
 217 simulations, driven by the GEOS-FP assimilated meteorological data, include detailed  
 218 tropospheric Ozone- $NO_x$ -VOCs- $HO_x$ -aerosol chemistry. More details are shown in  
 219 Yan et al. (2019). In the models, anthropogenic and natural sources are fully considered



in GEOS-Chem. Table S1 and Table S2 show a list of emission inventories in the global model and nested simulation, respectively. In China, the monthly grid data of  $0.25^\circ \times 0.25^\circ$  from MEIC inventory (<http://meicmodel.org>) for CO, NO<sub>x</sub>, SO<sub>2</sub> and non-methane volatile organic compounds (NMVOCs) in 2013-2014 is used. Over Central China, anthropogenic sources of these species are from our group SEEA (Source Emission and Environment Research) inventory with the grid data of  $0.1^\circ \times 0.1^\circ$  (not shown). The SEEA emission inventory was developed based on the year of 2017 for the Wuhan city cluster and it has been successfully adopted for the air quality simulating and forecasting of 7th CISM Military World Games in 2019. Other emission descriptions are shown in Supplementary Sect. S1.

In order to better simulate the spatiotemporal distribution of PM<sub>2.5</sub> over Central China, especially in winter heavy pollution periods, the standard v11-01 of GEOS-Chem is optimized according to the actual situation in China (see details in Supplementary Sect. S2), including optimizing PM<sub>2.5</sub> sources and increasing the proportion of sulfate primary emission (Yan et al., 2020). The PM<sub>2.5</sub> primary anthropogenic emissions enhance the PM<sub>2.5</sub> concentrations over Central China by 5-20  $\mu\text{g}/\text{m}^3$  in winter (Fig. S4). Compared with the results before the model optimization (Fig. S5), the sulfate concentration simulated by the optimized model increased from 10-20  $\mu\text{g}/\text{m}^3$  to 30-50  $\mu\text{g}/\text{m}^3$ . Further comparisons of PM<sub>2.5</sub> with observations and inorganic salts (sulfate, nitrate and ammonium) with reported values from previous studies are shown in Sect.3.3.

### 3. Results and Discussion

#### 3.1 Classification of PSCs

As shown in Fig. 2, among the circulation patterns of pollution-day at Jingzhou from 2013 to 2018, the frequency of SW-type circulation is the highest, accounting for 29% of the total pollution days. The frequencies of NW-type, A-type and C-type are also high, accounting for 27%, 19% and 12%, respectively. While the other six

circulation patterns are less occurred, with the frequencies less than 5%. Thus, the above four typical circulation types are considered as the main potential synoptic controls of the severe particle pollution episodes over Central China.

Figure 2

### 3.2 Characteristics of the four main PSCs

SW-type circulation is the predominant PSC of severe PM<sub>2.5</sub> pollution episodes. The circulation at 500 hPa is relatively flat and the whole East Asia region is affected by the westerly flow (Fig. S6a). Westerly belt fluctuates greatly at 700 hPa and there are two ridges and a southwest trough in the middle latitudes of Asia (Fig. S7a). Jingzhou is located in the front of a trough, prevailing the weak southwest airflow. At 850 hPa, the cold high pressure center is formed in Xinjiang of China. Warm low pressure appears in the low latitude area and weak high pressure appears in the East China Sea (Fig. 3a). In combination with the surface field, a high-low-high saddle like field forms from west to east (Fig. 4a). Such synoptic type is also the dominant weather system of eastern China (Shu et al., 2017; Yang et al., 2018). Jingzhou is located in the back of Bohai-northeast high pressure and the front of southwest warm low pressure. Thus it is affected by the southerly airflow, which could be conducive to the transport of air pollutants formed over southern China to Central China. Associated with small local surface wind speed (< 3 m/s) at Jingzhou, the dispersion of local and transported pollutants is inhibited.

Figure 3

NW-type circulation mainly occurs in the early winter (December and January). This synoptic pattern is also reported as one of the main types to affect the aerosol distributions over eastern China (Zheng et al., 2015). Circulation at 500 hPa is

controlled by one trough and one ridge, with the weak ridge located in the northwest of China and the shallow trough located in the northeast of China (Fig. S6b). The whole East Asia is affected by the westerly current. The trough and ridge at 700 hPa are deepened. Jingzhou is located at the bottom of the shallow trough, prevailing the west-northwest airflow, affected by the flow around the plateau (Fig. S7b). At 850 hPa, the cold high pressure center is formed in Xinjiang, and Jingzhou is affected by the northerly airflow, due to being in the front of the high pressure (Fig. 3b). For the sea level pressure, the cold high pressure is located in the west of Mongolia and Xinjiang of China (Fig. 4b). Jingzhou is located at the region with weak fluctuation in the front of the high pressure, and the surface wind speed is smaller than 2 m/s. The haze episodes induced by NW-type synoptic pattern is similar to the transmission-accumulation pollution caused by SW-type, but the transmission path is from Northern China to Central China.

Figure 4

A-type circulation also mainly occurs in the early winter. The high-altitude circulation field is controlled by one trough and one ridge (Fig. S6c and S7c). East Asia is affected by west-northwest air flow, and the SLP is controlled by a huge high pressure, with the center located in the southwest of Baikal Lake (Fig. 4c). A surface high pressure favors accumulation of air pollutants, especially over the regions of high pressure center (Leung et al., 2018). Jingzhou is in the sparse pressure field in front of the high pressure (Fig. 3c and 4c), with an average surface wind speed of  $\sim 1.3$  m/s. The uniform west-northwest air flow at high altitude would lead to the low water vapor content and less cloud amount, which is conducive to radiation cooling at night. In addition, due to the weak high pressure ridge in the north, it is not conducive to the eastward and southward movement of cold air, leading to the stable weather situation

and thus severe haze pollution at Jingzhou. This type is also responsible for most of the severe particulate pollution days in the BTH and YRD regions (Li et al., 2019).

C-type circulation mainly occurs in late winter and early spring, when the relative humidity is large with an average value of 74%. East Asia is controlled by the straight westerly flow, and the southwest shallow trough is obvious at 500 hPa (Fig. S6d). Additionally, the West Pacific subtropical high extends to the west, Central China is affected by the southwest flow. Southwest trough is deepened at 700 hPa, and Jingzhou is located in front of the trough and controlled by the southwest airflow (Fig. S7d). High pressure at the south of Xinjiang and the north of Plateau is strengthened at 850 hPa, and the southwest low pressure center is formed (Fig. 3d). Jingzhou is located in the low pressure system on the SLP field (Fig. 4d), with small surface wind speed (0-3 m/s). Together with the large relative humidity, which can promote the hygroscopic growth of particulate matter (Twohy et al., 2009; Zheng et al., 2015), the haze pollution is persistent and serious at Jingzhou. The impact of low-pressure systems on winter heavy air pollution have also been reported in the northwest Sichuan Basin (Ning et al., 2018).

### **3.3 PM<sub>2.5</sub> and chemical components under the four main PSCs in control simulations**

The spatiotemporal distribution of PM<sub>2.5</sub> and its components under the four typical synoptic controls over Central China were simulated by optimized GEOS-Chem model. In order to reduce the simulation cost, the continuous four severe haze episodes occurred during November, 2013-February, 2014 are selected. These four haze episodes are controlled by the synoptic pattern of SW-type (18-25 November, 2013), NW-type (19-26 December, 2013), A-type (14-21 January, 2014) and C-type (26 January - 2 February, 2014), respectively. The air quality at Jingzhou during the four pollution episodes is between grade 5 (PM<sub>2.5</sub> > 150 µg/m<sup>3</sup>) and grade 6 heavy pollution (PM<sub>2.5</sub> > 250 µg/m<sup>3</sup>, as Fig. 5a and S1a shown). The simulation time is started at

November 1st, 2013, with the first two weeks used as spin up to eliminate the impact of initial conditions.

Figure 5

Figure 6

The daily/hourly mean PM<sub>2.5</sub> concentrations at Jingzhou in the four typical heavy pollution processes simulated by the control (CON) simulation (Table 2) are compared with the observations (Fig. 5a/Fig. S1a). The model underestimates the observed PM<sub>2.5</sub> concentrations (by 43.3  $\mu\text{g}/\text{m}^3$  on average), especially in the high PM<sub>2.5</sub> periods (by 116.8  $\mu\text{g}/\text{m}^3$  at the maximum occurring in November 21-23, 2013). The possible causes for underestimation are meteorological field deviations (an overestimate in temperature and wind speed and an underestimate in humidity; Table S3) and emission errors. Anthropogenic emissions for PM<sub>2.5</sub> precursors used here are for the year 2017 over Central China from SEEA inventory (Table S4). From 2013 to 2017, anthropogenic NO<sub>x</sub>, SO<sub>2</sub>, and primary PM<sub>2.5</sub> emissions in Central China have declined substantially (Table S4), due to implementation of stringent emission control measures for the 12<sup>th</sup>-13<sup>th</sup> Five-Year Plans (Zheng et al., 2018). The anthropogenic emissions biases may affect our simulations and PM<sub>2.5</sub> attribution results to some extent. Additionally, the underestimation is on a national scale when compared with the MEE observations, with a bias of -29.3  $\mu\text{g}/\text{m}^3$ , -18.7  $\mu\text{g}/\text{m}^3$ , -39.0  $\mu\text{g}/\text{m}^3$  and -21.4  $\mu\text{g}/\text{m}^3$  on average for SW-type, NW-type, A-type and C-type synoptic controlled episodes, respectively (Fig. 6). The national negative biases may be also attributed to insufficient resolution of the model (Yan et al., 2014) and imperfect chemical mechanisms (Yan et al., 2019). Nevertheless, the model can reproduce the evolution of each severe particle pollution episode well, including the accumulation of pollutants, the continuing process and the gradual dissipation of pollution (Fig. 5a/Fig. S1a).

Table 2

In order to examine the model performances in the  $PM_{2.5}$  chemical compositions, we have reviewed the reported concentrations of  $PM_{2.5}$  and the three inorganic salts (sulfate, nitrate and ammonium) in other cities (Table 4). The contributions of sulfate, nitrate and ammonium are 9.1%-31.9%, 5.7%-32.1% and 5.9%-13.3%, respectively. Figure S8/S9 shows the modeled spatial distribution of  $PM_{2.5}$ , sulfate, nitrate and ammonium concentrations averaged in the four typical heavy pollution processes over Jingzhou/China. The fractions of each inorganic salt to  $PM_{2.5}$  for these four heavy pollution episodes are also shown in Fig. S10. Over Central China, the main components of  $PM_{2.5}$  are the three inorganic salts in these pollution episodes, with the averaged contributions of sulfate, nitrate and ammonium being ~20%, ~18% and ~13%, respectively (Table 3). Our modelling results are comparable to the previous observed results (Table 4). Huang et al. (2014) have also reported that the three secondary inorganic particles rank the highest fraction among the  $PM_{2.5}$  species in Central-Eastern China. As shown in Table 3, in addition to inorganic salts, other chemical components include dust (~15%), black carbon (~7%), primary organic aerosol (~14%) and second organic aerosol (~13%). In these four pollution events, the differences in mass percentages of each chemical component ranged from 0.1% (dust) to 6.2% (sulfate) (Table 3). See details in Sect. 3.4 for further analysis of the causes for the differences.

Table 3

Table 4

### 3.4 Local emissions versus transmission contributions to $PM_{2.5}$ under the four main PSCs

In order to investigate the effectiveness of emission control to reduce  $PM_{2.5}$  pollution of Central China in the four typical severe particle pollution episodes, firstly

we estimate the local sources versus transmission contributions of  $PM_{2.5}$  by GEOS-Chem sensitivity simulations (Table 2). Results of XJ0 (Emissions outside Jingzhou are zero) indicates the contribution of local emission sources to the  $PM_{2.5}$  pollution over Jingzhou. The difference between CON and XCC0 (Emissions outside Central China are zero) shows the transmission contribution of  $PM_{2.5}$  outside Central China to Jingzhou. The difference between CON and NCP0/YRD0/PRD0/SCB0 (Emissions over NCP/YRD/PRD/SCB are zero) represents the contribution of pollution transport from NCP/YRD/PRD/SCB regions to Jingzhou.

Figure 7

For the SW-type synoptic situation, differences between the simulation results of NCP0/YRD0/SCB0 and CON show that pollution controlled by SW-type circulation over Central China is almost not affected by the emission sources from North China/East China/Sichuan Basin. The concentrations of  $PM_{2.5}$  and three inorganic salts simulated by NCP0/YRD0/SCB0 are similar to those simulated by CON, with a difference less than 3.0% (Fig. 8). However, affected by the southerly airflow at 850 hPa (Fig. 7), air pollutants formed over southern China could be transmitted to Central China, with the transport contribution of 7.6%. In addition, the contributions from transboundary transport from non-Jingzhou Central China is simulated to be 12.0% by comparing the results of XJ0 and XCC0. The transport of air pollutants from the south leads to the smallest proportion of the three inorganic salts (45.7%) in Jingzhou among the four pollution episodes (50.3%-55.5% for other three episodes), because the emissions of  $SO_2$ ,  $NO_2$  and  $NH_3$  in the south (especially in Guangxi and Guizhou province) are smaller than those in Central China (Li et al., 2017a). Associated with the small surface wind speed of 2.1 m/s on average (Fig. 5) and the weak ascending in the vertical direction (Fig. 7) at Jingzhou, it is not conducive to the dispersion of local pollutants (Zheng et al., 2015). The high  $PM_{2.5}$  concentrations are mainly accumulated

by local emissions. The simulations of XJ0 and CON show that local emission sources over Jingzhou contribute ~70% to PM<sub>2.5</sub>.

Figure 8

Figure 9

For the NW-type synoptic mode, affected by the northerly airflow (Fig. 9), it is conducive to the southward movement of air pollutants in northern China (He et al., 2018; Leung et al., 2018). Influenced by the local and surrounding terrain over Central China (Fig. 1), two transmission channels are formed from north to south and from northeast to southwest (Fig. 9). In addition, due to the local small wind speed (1.4 m/s on average) near the ground (Fig. 5), the weak convection and the warm ridge along the East Asia coast (Fig. 9), the local and transported pollutants accumulate in Central China. The average concentration of PM<sub>2.5</sub> in Jingzhou is 179.4 µg/m<sup>3</sup>. Due to the transport contribution of pollutants from northern China (with much higher anthropogenic emissions of SO<sub>2</sub>, NO<sub>2</sub> and NH<sub>3</sub>) (Li et al., 2017a), the total proportion of the three inorganic salts is the highest (55.5%). The PM<sub>2.5</sub> concentration simulated in NCP0 is 63.1% of that by CON simulation (Fig. 8), indicating that the transmission contribution from North China in this heavy pollution episode is as high as 36.9%. The contribution of local emission sources is much smaller than that of SW-type synoptic pattern, only 41.2% (comparison between XJ0 and CON).

Figure 10

Under the A-type circulation, Jingzhou is controlled by a high pressure system (Fig. 10) which can lead to stable weather conditions caused by radiation inversion (Guo et al., 2015) and subsidence inversion (Kurita et al., 1985), being favorable to continuous accumulation of local pollutants (Guo et al., 2015). The distribution of PM<sub>2.5</sub>



in China is similar to that of SW-type weather condition, with an averaged  $\text{PM}_{2.5}$  concentration of  $128.6 \mu\text{g}/\text{m}^3$  over Central China. Unlike SW-type, the  $\text{PM}_{2.5}$  at Jingzhou in this synoptic pattern is less affected by transboundary transport, with the total transport contribution of the surrounding four major pollution regions being less than 9%. The contribution of local emission sources is about 82% (Fig. 8).

Figure 11

Under the C-type synoptic pattern, the southwest low pressure center is formed at 850 hPa, and Jingzhou is located in the low pressure system of the SLP field (Fig. 11). In combination with the large relative humidity (78% on average; Fig. 5; because that the occurrence season of C-type is the late winter and early spring), it can promote the haze pollution due to its impact on hydrophilic aerosols (Twohy et al., 2009; Zheng et al., 2015). Together with the small wind speed (less than 4 m/s; Fig. 5), it is easy to cause the accumulation of pollutants. The average concentration of  $\text{PM}_{2.5}$  over Central China is as high as  $203.7 \mu\text{g}/\text{m}^3$ . Air pollution controlled by this weather condition is the most serious of the four typical synoptic controls. However, in this weather situation, pollutants in North China are easy to diffuse (Miao et al., 2017; Li et al., 2019), and the concentration of  $\text{PM}_{2.5}$  is significantly lower than that in the former three weather situations (Fig. 11 and Fig. S9). The contribution of pollution transport from non-Central China region simulated by GEOS-Chem is less than 8%, and the contribution of local emission sources at Jingzhou is more than 85% (Fig. 7).

### 3.5 Effectiveness of emission reduction under the four main PSCs

In order to estimate the effectiveness of emission reduction in severe pollution events forced by the four potential synoptic controls, we conduct sensitivity simulations by applying seven emission scenarios (Table 2). All emission scenarios use the reduction ratio of 20% which is close to the average of the target emission reduction of

all provinces in the 13<sup>th</sup> Five-year plan (The State Council of the People's Republic of China, 2016). Although the base year of emission reduction is 2015 for the 13<sup>th</sup> Five-year plan, it does not affect to use the simulation results of emission scenarios (with the reduction ratio of 20% applied to the simulated year 2013/2014) to explore the emission reduction effect of specific haze pollution events. The differences in model results between CON (control simulation) and JSN/JSNN/JALL (emissions of SO<sub>2</sub>+NO<sub>x</sub>/SO<sub>2</sub>+NO<sub>x</sub>+NH<sub>3</sub>/all pollution sources at Jingzhou are reduced by 20%) represent the environmental benefits caused by different local emission reduction scenarios. The potential PM<sub>2.5</sub> mitigations by joint prevention and control in different regions are calculated by sensitivity experiments of CCALL (emissions of all pollution sources over Central China are reduced by 20%), CNALL (over Central China and NCP region), CPALL (over Central China and PRD region) and TALL (over Central China, NCP, YRD, PRD and SCB regions).

In the JSN emission reduction scenario, the sulfate and ammonium concentrations over Jingzhou are significantly reduced by 3.2-5.8 µg/m<sup>3</sup> (12.7-14.5%) and 0.6-1.9 µg/m<sup>3</sup> (3.2-5.9%) in these four pollution events, respectively. However, the concentration of nitrate increases (1.3-1.7%). This is because there is a competition mechanism between nitrate and sulfate. Ammonium ions always react with sulfate ions first to generate ammonium sulfate, which will continue to react with nitrate ions to generate ammonium nitrate when ammonium ions are rich (Mao et al., 2010). Thus the reduction of SO<sub>2</sub> emission increases the concentration of nitrate, which offset the contribution of sulfate particle reduction to the environment to some extent. Therefore, the application of JSN emission reduction scheme only reduces the PM<sub>2.5</sub> concentrations by 3.1-7.2 µg/m<sup>3</sup> (2.0-3.5%, Fig. 12). This inefficient emission reduction scheme is most widely used in heavy pollution areas over China in the past decade, ignoring the synergistic effect of various precursors.

Figure 12

498

499 By applying the JSNN and JALL emission reduction scenarios, we aim to evaluate  
500 the synergistic effect of multiple precursors on emission reduction. These two scenarios  
501 reduce the average sulfate concentration in Jingzhou by 2.8-6.7  $\mu\text{g}/\text{m}^3$  (11.3-17.3%)  
502 and 2.9-7.2  $\mu\text{g}/\text{m}^3$  (11.7-17.9%), and the ammonium concentration by 2.0-4.8  $\mu\text{g}/\text{m}^3$   
503 (12.1-16.5%) and 2.2-4.7  $\mu\text{g}/\text{m}^3$  (13.2-17.3%), respectively. Unlike the increments of  
504 nitrate in JSN emission reduction scenario, the nitrate decreases (JSNN: 0.3-1.2  $\mu\text{g}/\text{m}^3$ ;  
505 JALL: 0.4-1.5  $\mu\text{g}/\text{m}^3$ ). Therefore, through the application of JSNN and JALL emission  
506 reduction schemes,  $\text{PM}_{2.5}$  concentrations decrease by 4.9-8.3% and 9.0-15.9%,  
507 respectively (Fig. 12), much higher than the improvement by JSN scenario. Zheng et  
508 al. (2019b) has also evaluated the sensitiveness of  $\text{NH}_3$  control to  $\text{PM}_{2.5}$  reduction based  
509 on observations. However, these results indicate that it is unrealistic to substantially  
510 reduce local emissions to achieve the national air quality standard in the long term.

511 Additionally, the sensitivity simulations by excluding emission sources over  
512 upwind regions are conducted to estimate the potential  $\text{PM}_{2.5}$  mitigations of inter-  
513 regional and intra-regional joint control. Our results show that after applying TALL  
514 emission reduction scenario,  $\text{PM}_{2.5}$  concentrations have been significantly improved,  
515 with the improvement rates increased from 9.0-15.9% (by JALL scenario) to 17.4-18.8%  
516 (Fig. 12). Especially, the NW-type synoptic controlled air pollution episode shows the  
517 best effect of joint prevention, followed by SW-type. For NW-type, by reducing  
518 emissions over Central China and Northern China (CNALL scheme),  $\text{PM}_{2.5}$   
519 concentrations are reduced by 26.5  $\mu\text{g}/\text{m}^3$  (16.9%), much more effective than JALL  
520 emission reduction scheme (14.1  $\mu\text{g}/\text{m}^3$ , 9.0%). In SW-type controlled pollution  
521 episode, it should be otherwise to decrease the emissions over Southern China in  
522 addition to Central China.

523

#### 524 4. Conclusion

The PM<sub>2.5</sub> pollution in autumn and winter haze periods is now the key obstacle for further improving air quality in China. The extremely severe and persistent PM<sub>2.5</sub> pollution episodes are attributed to adverse synoptic conditions in addition to high precursor emissions. For the PM<sub>2.5</sub> mitigations during winter haze episodes in specific region forced by various potential synoptic controls, how to effectively reduce emissions has become an urgent scientific question to be answered. Our results over Central China could provide reference for regional air quality policy-making.

Through Lamb-Jenkenson circulation classification, the top four potential synoptic controls of heavy PM<sub>2.5</sub> pollution days (totally 109 days) over Central China from 2013 to 2018 are decomposed to be SW-type, NW-type A-type and C-type, accounting for 29%, 27%, 19% and 12% of the total pollution days, respectively. In these four PSCs, three inorganic salt aerosols (sulfate: ~20%; nitrate: ~18%; ammonium: ~13%) totally accounted for ~51% of PM<sub>2.5</sub> concentrations simulated by optimized GEOS-Chem modelling.

In the SW-type/NW-type synoptic situation, affected by the southerly/northerly airflow, pollutants over southern/northern China could be transmitted to Central China, with the transport contribution of 7.6%/37%. In the situation A-type/C-type weather, affected by stable weather condition/high relative humidity, the pollution processes are less affected by the emission sources from non-local regions. And the local emission sources dominate the contribution (82%/85%) to PM<sub>2.5</sub>.

By only reducing SO<sub>2</sub> and NO<sub>x</sub> emission and not controlling NH<sub>3</sub>, due to the competition mechanism between nitrate and sulfate, the concentrations of sulfate and ammonium decrease, but the concentration of nitrate increases instead. The enhanced nitrate counteracts the effect of sulfate reduction on PM<sub>2.5</sub> mitigations, with less than 4% decrease in PM<sub>2.5</sub>. Even if the NH<sub>3</sub> emission is also reduced, the PM<sub>2.5</sub> concentration reduction is less than 9%. By applying the TALL emission reduction scenario, PM<sub>2.5</sub> concentrations would decrease significantly, with the improvement rate increased from 9.0-15.9% (by JALL scenario) to 17.4-18.8%.

These results provide an opportunity to effectively mitigate haze pollution by local emission control actions in coordination with regional collaborative actions according to different synoptic patterns. Especially, the NW-type synoptic controlled air pollution episode shows the best effect of joint prevention, followed by SW-type. It is noted that in this study, the division of transmission areas is relatively rough, and more accurate source area identification and refined assessment of emission reduction effect of multiple pollutants from source groups are needed in the follow-up.

### **Acknowledgement**

This study was financially supported by the National Natural Science Foundation of China (41830965; 41775115; 41905112), the Key Program of Ministry of Science and Technology of the People's Republic of China (2017YFC0212602; 2016YFA0602002), the Key Program for Technical Innovation of Hubei Province (2017ACA089), the Program for Environmental Protection in Hubei Province (2017HB11) and the China Postdoctoral Science Foundation funded project (258572). The research was also funded by the Fundamental Research Funds for the Central Universities, China University of Geosciences (Wuhan) (G1323519230; 201616; 26420180020; CUG190609) and the Start-up Foundation for Advanced Talents (162301182756).

### **Author contributions**

Yingying Yan and Shaofei Kong conceived and designed the research. Yingying Yan performed the data processing, model simulations, and analyses. Yue Zhou assisted in the circulation classification. Jian Wu provided the emission data over Central China. Shaofei Kong, Tianliang Zhao and Dantong Liu contributed the funding acquisition. Yingying Yan wrote the paper with input from all authors.

### **Data availability**

Observational data are obtained from individual sources (see links in the text).  
Model results are available upon request. Model codes are available on a collaborative basis.

## Competing interests

The authors declare that they have no conflict of interest.

## References

- The People's Government of Beijing Municipality (PGBM): Emergency plan for severe air pollution in Beijing, available at: [http://www.beijing.gov.cn/zhengce/zhengcefagui/201905/t20190522\\_61613.html](http://www.beijing.gov.cn/zhengce/zhengcefagui/201905/t20190522_61613.html) (last access: 14 July 2018), 2018 (in Chinese).
- The People's Government of Guangdong Province (PGGP): Emergency plan for severe air pollution in Pearl River Delta, available at: [http://www.gd.gov.cn/gkmlpt/content/0/142/post\\_142657.html#7](http://www.gd.gov.cn/gkmlpt/content/0/142/post_142657.html#7) (last access: 14 July 2018), 2014 (in Chinese).
- The People's Government of Shanghai Municipality (PGSM): Special emergency plan for heavy air pollution in Shanghai, available at: <http://www.shanghai.gov.cn/nw2/nw2314/nw2319/nw31973/nw32019/nw32022/nw32023/u21aw1316153.html> (last access: 14 July 2018), 2018 (in Chinese).
- The State Council of the People's Republic of China (SCPPC): The Thirteenth Five-Year Plan for Energy Saving and Emission Reduction, available at: [http://www.gov.cn/gongbao/content/2017/content\\_5163448.htm](http://www.gov.cn/gongbao/content/2017/content_5163448.htm) (last access: 14 July 2018), 2016 (in Chinese).
- The State Council of the People's Republic of China (SCPPC): Air Pollution Prevention and Control Action Plan, available at: [http://www.gov.cn/zhengce/content/2013-09/13/content\\_4561.htm](http://www.gov.cn/zhengce/content/2013-09/13/content_4561.htm) (last access: 14 July 2018), 2013 (in Chinese).
- Jenkinson A. F., Collison F. P.: An initial climatology of gales over the North Sea. Synoptic Climatology Branch Memorandum, 62. Bracknell: Meteorological Office, 1-18, 1977.
- Lamb H H. Types and spells of weather around the year in the British Isles. Quarterly Journal Royal Meteorological Society, 76, 393-438, 1950.
- Agarwal, N. K., Sharma, P., and Agarwal, S. K.: Particulate matter air pollution and cardiovascular disease, Medical Science, 21, 270-279, 2017.

615 An, Z., Huang, R.J., Zhang, R., Tie, X., Li, G., Cao, J., Zhou, W., Shi, Z., Han, Y., Gu,  
 616 Z., and Ji, Y.: Severe haze in northern China: A synergy of anthropogenic emissions  
 617 and atmospheric processes, *Proceedings of the National Academy of Sciences of the*  
 618 *United States of America*, 116, 8657-8666, 10.1073/pnas.1900125116, 2019.  
 619 Bei, N., Zhao, L., Xiao, B., Meng, N., and Feng, T.: Impacts of local circulations on the  
 620 wintertime air pollution in the Guanzhong Basin, China, *Science of the Total*  
 621 *Environment*, 592, 373-390, 10.1016/j.scitotenv.2017.02.151, 2017.  
 622 Bi, X., Dai, Q., Wu, J., Zhang, Q., Zhang, W., Luo, R., Cheng, Y., Zhang, J., Wang, L.,  
 623 Yu, Z., Zhang, Y., Tian, Y., and Feng, Y.: Characteristics of the main primary source  
 624 profiles of particulate matter across China from 1987 to 2017, *Atmospheric*  
 625 *Chemistry and Physics*, 19, 3223-3243, 10.5194/acp-19-3223-2019, 2019.  
 626 Cheng, J., Su, J., Cui, T., Li, X., Dong, X., Sun, F., Yang, Y., Tong, D., Zheng, Y., Li,  
 627 Y., Li, J., Zhang, Q., and He, K.: Dominant role of emission reduction in PM<sub>2.5</sub> air  
 628 quality improvement in Beijing during 2013-2017: a model-based decomposition  
 629 analysis, *Atmospheric Chemistry and Physics*, 19, 6125-6146, 10.5194/acp-19-  
 630 6125-2019, 2019.  
 631 Cheng, Z., Luo, L., Wang, S., Wang, Y., Sharma, S., Shimadera, H., Wang, X., Bressi,  
 632 M., de Miranda, R. M., Jiang, J., Zhou, W., Fajardo, O., Yan, N., and Hao, J.: Status  
 633 and characteristics of ambient PM<sub>2.5</sub> pollution in global megacities, *Environment*  
 634 *International*, 89-90, 212-221, 10.1016/j.envint.2016.02.003, 2016.  
 635 Chuang, M.T., Chiang, P.C., Chan, C.C., Wang, C.F., Chang, E. E., and Lee, C.T.: The  
 636 effects of synoptical weather pattern and complex terrain on the formation of aerosol  
 637 events in the Greater Taipei area, *Science of the Total Environment*, 399, 128-146,  
 638 10.1016/j.scitotenv.2008.01.051, 2008.  
 639 Geng, G., Xiao, Q., Zheng, Y., Tong, D., Zhang, Y., Zhang, X., Zhang, Q., He, K., and  
 640 Liu, Y.: Impact of China's Air Pollution Prevention and Control Action Plan on PM<sub>2.5</sub>  
 641 chemical composition over eastern China, *Science China-Earth Sciences*, 62, 1872-  
 642 1884, 10.1007/s11430-018-9353-x, 2019.  
 643 Gong, W., Zhang, T., Zhu, Z., Ma, Y., Ma, X., and Wang, W.: Characteristics of PM<sub>1.0</sub>,  
 644 PM<sub>2.5</sub>, and PM<sub>10</sub>, and Their Relation to Black Carbon in Wuhan, Central China,  
 645 *Atmosphere*, 6, 1377-1387, 10.3390/atmos6091377, 2015.  
 646 Guo, L., Guo, X., Fang, C., and Zhu, S.: Observation analysis on characteristics of  
 647 formation, evolution and transition of a long-lasting severe fog and haze episode in  
 648 North China, *Science China-Earth Sciences*, 58, 329-344, 10.1007/s11430-014-  
 649 4924-2, 2015.  
 650 He, J., Gong, S., Zhou, C., Lu, S., Wu, L., Chen, Y., Yu, Y., Zhao, S., Yu, L., and Yin,  
 651 C.: Analyses of winter circulation types and their impacts on haze pollution in

Beijing, Atmospheric Environment, 192, 94-103, 10.1016/j.atmosenv.2018.08.060, 2018.

Huang, R.J., Zhang, Y., Bozzetti, C., Ho, K.F., Cao, J.J., Han, Y., Daellenbach, K. R., Slowik, J. G., Platt, S. M., Canonaco, F., Zotter, P., Wolf, R., Pieber, S. M., Bruns, E. A., Crippa, M., Ciarelli, G., Piazzalunga, A., Schwikowski, M., Abbaszade, G., Schnelle-Kreis, J., Zimmermann, R., An, Z., Szidat, S., Baltensperger, U., El Haddad, I., and Prevot, A. S. H.: High secondary aerosol contribution to particulate pollution during haze events in China, *Nature*, 514, 218-222, 10.1038/nature13774, 2014.

Huang, X., Ding, A., Gao, J., Zheng, B., Zhou, D., Qi, X., Tang, R., Wang, J., Ren, C., Nie, W., Chi, X., Xu, Z., Chen, L., Li, Y., Che, F., Pang, N., Wang, H., Tong, D., Qin, W., Cheng, W., Liu, W., Fu, Q., Liu, B., Chai, F., Davis, S. J., Zhang, Q., and He, K.: Enhanced secondary pollution offset reduction of primary emissions during COVID-19 lockdown in China, *National Science Review*, 10.1093/nsr/nwaa137, 2020.

Kurita, H., Sasaki, K., Muroga, H., Ueda, H., and Wakamatsu, S.: Long-range transport of air pollution under light gradient wind conditions, *Journal of Climate and Applied Meteorology*, 24, 425-434, 10.1175/1520-0450(1985)024<0425:lroap>2.0.co;2, 1985.

Leung, D. M., Tai, A. P. K., Mickley, L. J., Moch, J. M., van Donkelaar, A., Shen, L., and Martin, R. V.: Synoptic meteorological modes of variability for fine particulate matter (PM<sub>2.5</sub>) air quality in major metropolitan regions of China, *Atmospheric Chemistry and Physics*, 18, 6733-6748, 10.5194/acp-18-6733-2018, 2018.

Li, J., Liao, H., Hu, J., and Li, N.: Severe particulate pollution days in China during 2013-2018 and the associated typical weather patterns in Beijing-Tianjin-Hebei and the Yangtze River Delta regions, *Environmental Pollution*, 248, 74-81, 10.1016/j.envpol.2019.01.124, 2019.

Li, M., Zhang, Q., Kurokawa, J.-i., Woo, J.-H., He, K., Lu, Z., Ohara, T., Song, Y., Streets, D. G., Carmichael, G. R., Cheng, Y., Hong, C., Huo, H., Jiang, X., Kang, S., Liu, F., Su, H., and Zheng, B.: MIX: a mosaic Asian anthropogenic emission inventory under the international collaboration framework of the MICS-Asia and HTAP, *Atmospheric Chemistry and Physics*, 17, 935-963, 10.5194/acp-17-935-2017, 2017a.

Li, X., Zhang, Q., Zhang, Y., Zhang, L., Wang, Y., Zhang, Q., Li, M., Zheng, Y., Geng, G., Wallington, T. J., Han, W., Shen, W., and He, K.: Attribution of PM<sub>2.5</sub> exposure in Beijing-Tianjin-Hebei region to emissions: implication to control strategies, *Science Bulletin*, 62, 957-964, 10.1016/j.scib.2017.06.005, 2017b.



- Li, Z., Guo, J., Ding, A., Liao, H., Liu, J., Sun, Y., Wang, T., Xue, H., Zhang, H., and Zhu, B.: Aerosol and boundary-layer interactions and impact on air quality, *National Science Review*, 4, 810-833, 10.1093/nsr/nwx117, 2017c.
- Liao, Z., Gao, M., Sun, J., and Fan, S.: The impact of synoptic circulation on air quality and pollution-related human health in the Yangtze River Delta region, *Science of the Total Environment*, 607, 838-846, 10.1016/j.scitotenv.2017.07.031, 2017.
- Liao, Z., Xie, J., Fang, X., Wang, Y., Zhang, Y., Xu, X., and Fan, S.: Modulation of synoptic circulation to dry season PM<sub>2.5</sub> pollution over the Pearl River Delta region: An investigation based on self-organizing maps, *Atmospheric Environment*, 230, 10.1016/j.atmosenv.2020.117482, 2020.
- Lin, Y., Zou, J., Yang, W., and Li, C.Q.: A Review of Recent Advances in Research on PM<sub>2.5</sub> in China, *International Journal of Environmental Research and Public Health*, 15, 10.3390/ijerph15030438, 2018.
- Liu, M., Huang, X., Song, Y., Tang, J., Cao, J., Zhang, X., Zhang, Q., Wang, S., Xu, T., Kang, L., Cai, X., Zhang, H., Yang, F., Wang, H., Yu, J. Z., Lau, A. K. H., He, L., Huang, X., Duan, L., Ding, A., Xue, L., Gao, J., Liu, B., and Zhu, T.: Ammonia emission control in China would mitigate haze pollution and nitrogen deposition, but worsen acid rain, *Proceedings of the National Academy of Sciences of the United States of America*, 116, 7760-7765, 10.1073/pnas.1814880116, 2019.
- Mao, J., Jacob, D. J., Evans, M. J., Olson, J. R., Ren, X., Brune, W. H., Clair, J. M. S., Crounse, J. D., Spencer, K. M., Beaver, M. R., Wennberg, P. O., Cubison, M. J., Jimenez, J. L., Fried, A., Weibring, P., Walega, J. G., Hall, S. R., Weinheimer, A. J., Cohen, R. C., Chen, G., Crawford, J. H., McNaughton, C., Clarke, A. D., Jaeglé, L., Fisher, J. A., Yantosca, R. M., Le Sager, P., and Carouge, C.: Chemistry of hydrogen oxide radicals (HOx) in the Arctic troposphere in spring, *Atmospheric Chemistry and Physics*, 10, 5823-5838, 10.5194/acp-10-5823-2010, 2010.
- Miao, Y., Guo, J., Liu, S., Liu, H., Li, Z., Zhang, W., and Zhai, P.: Classification of summertime synoptic patterns in Beijing and their associations with boundary layer structure affecting aerosol pollution, *Atmospheric Chemistry and Physics*, 17, 3097-3110, 10.5194/acp-17-3097-2017, 2017.
- Ning, G., Wang, S., Yim, S. H. L., Li, J., Hu, Y., Shang, Z., Wang, J., and Wang, J.: Impact of low-pressure systems on winter heavy air pollution in the northwest Sichuan Basin, China, *Atmospheric Chemistry and Physics*, 18, 13601-13615, 10.5194/acp-18-13601-2018, 2018.
- Pope, R. J., Savage, N. H., Chipperfield, M. P., Ordonez, C., and Neal, L. S.: The influence of synoptic weather regimes on UK air quality: regional model studies of

725 tropospheric column NO<sub>2</sub>, *Atmospheric Chemistry and Physics*, 15, 11201-11215,  
 726 10.5194/acp-15-11201-2015, 2015.

727 Russo, A., Trigo, R. M., Martins, H., and Mendes, M. T.: NO<sub>2</sub>, PM<sub>10</sub> and O<sub>3</sub> urban  
 728 concentrations and its association with circulation weather types in Portugal,  
 729 *Atmospheric Environment*, 89, 768-785, 10.1016/j.atmosenv.2014.02.010, 2014.

730 Shu, L., Xie, M., Gao, D., Wang, T., Fang, D., Liu, Q., Huang, A., and Peng, L.:  
 731 Regional severe particle pollution and its association with synoptic weather patterns  
 732 in the Yangtze River Delta region, China, *Atmospheric Chemistry and Physics*, 17,  
 733 12871-12891, 10.5194/acp-17-12871-2017, 2017.

734 Sun, Y., Niu, T., He, J., Ma, Z., Liu, P., Xiao, D., Hu, J., Yang, J., and Yan, X.:  
 735 Classification of circulation patterns during the formation and dissipation of  
 736 continuous pollution weather over the Sichuan Basin, China, *Atmospheric*  
 737 *Environment*, 223, 10.1016/j.atmosenv.2019.117244, 2020.

738 Sun, Y. L., Chen, C., Zhang, Y. J., Xu, W. Q., Zhou, L. B., Cheng, X. L., Zheng, H. T.,  
 739 Ji, D. S., Li, J., Tang, X., Fu, P. Q., and Wang, Z. F.: Rapid formation and evolution  
 740 of an extreme haze episode in Northern China during winter 2015, *Scientific Reports*,  
 741 6, 10.1038/srep27151, 2016.

742 Tian, S. L., Pan, Y. P., and Wang, Y. S.: Size-resolved source apportionment of  
 743 particulate matter in urban Beijing during haze and non-haze episodes, *Atmospheric*  
 744 *Chemistry and Physics*, 16, 1-19, 10.5194/acp-16-1-2016, 2016.

745 Trigo, R. M., and DaCamara, C. C.: Circulation weather types and their influence on  
 746 the precipitation regime in Portugal, *International Journal of Climatology*, 20, 1559-  
 747 1581, 10.1002/1097-0088(20001115)20:13<1559::aid-joc555>3.0.co;2-5, 2000.

748 Twohy, C. H., Coakley, J. A., Jr., and Tahnk, W. R.: Effect of changes in relative  
 749 humidity on aerosol scattering near clouds, *Journal of Geophysical Research-*  
 750 *Atmospheres*, 114, 10.1029/2008jd010991, 2009.

751 Wang, X., Wei, W., Cheng, S., Li, J., Zhang, H., and Lv, Z.: Characteristics and  
 752 classification of PM<sub>2.5</sub> pollution episodes in Beijing from 2013 to 2015, *Science of*  
 753 *the Total Environment*, 612, 170-179, 10.1016/j.scitotenv.2017.08.206, 2018.

754 Wang, Y., Chen, Y., Wu, Z., Shang, D., Bian, Y., Du, Z., Schmitt, S. H., Su, R.,  
 755 Gkatzelis, G. I., Schlag, P., Hohaus, T., Voliotis, A., Lu, K., Zen, L., Zhao, C.,  
 756 Alfarra, M. R., McFiggans, G., Wiedensohler, A., Kiendler-Scharr, A., Zhang, Y.,  
 757 and Hu, M.: Mutual promotion between aerosol particle liquid water and particulate  
 758 nitrate enhancement leads to severe nitrate-dominated particulate matter pollution  
 759 and low visibility, *Atmospheric Chemistry and Physics*, 20, 2161-2175, 10.5194/acp-  
 760 20-2161-2020, 2020.

- Wu, J., Kong, S., Wu, F., Cheng, Y., Zheng, S., Yan, Q., Zheng, H., Yang, G., Zheng, M., Liu, D., Zhao, D., and Qi, S.: Estimating the open biomass burning emissions in central and eastern China from 2003 to 2015 based on satellite observation, *Atmospheric Chemistry and Physics*, 18, 11623-11646, 10.5194/acp-18-11623-2018, 2018.
- Xu, G., Jiao, L., Zhang, B., Zhao, S., Yuan, M., Gu, Y., Liu, J., and Tang, X.: Spatial and temporal variability of the PM<sub>2.5</sub>/PM<sub>10</sub> ratio in Wuhan, Central China, *Aerosol and Air Quality Research*, 17, 741-751, 10.4209/aaqr.2016.09.0406, 2017.
- Yan, Q., Kong, S., Yan, Y., Liu, H., Wang, W., Chen, K., Yin, Y., Zheng, H., Wu, J., Yao, L., Zeng, X., Cheng, Y., Zheng, S., Wu, F., Niu, Z., Zhang, Y., Zheng, M., Zhao, D., Liu, D., and Qi, S.: Emission and simulation of primary fine and submicron particles and water-soluble ions from domestic coal combustion in China, *Atmospheric Environment*, 224, 10.1016/j.atmosenv.2020.117308, 2020.
- Yan, Y., Cabrera-Perez, D., Lin, J., Pozzer, A., Hu, L., Millet, D. B., Porter, W. C., and Lelieveld, J.: Global tropospheric effects of aromatic chemistry with the SAPRC-11 mechanism implemented in GEOS-Chem version 9-02, *Geoscientific Model Development*, 12, 111-130, 10.5194/gmd-12-111-2019, 2019.
- Yan, Y. Y., Lin, J. T., Kuang, Y., Yang, D., and Zhang, L.: Tropospheric carbon monoxide over the Pacific during HIPPO: two-way coupled simulation of GEOS-Chem and its multiple nested models, *Atmospheric Chemistry and Physics*, 14, 12649-12663, 10.5194/acp-14-12649-2014, 2014.
- Yang, Y., Zheng, X., Gao, Z., Wang, H., Wang, T., Li, Y., Lau, G. N. C., and Yim, S. H. L.: Long-term trends of persistent synoptic circulation events in planetary boundary layer and their relationships with haze pollution in winter half year over Eastern China, *Journal of Geophysical Research-Atmospheres*, 123, 10991-11007, 10.1029/2018jd028982, 2018.
- Yu, C., Zhao, T., Bai, Y., Zhang, L., Kong, S., Yu, X., He, J., Cui, C., Yang, J., You, Y., Ma, G., Wu, M., and Chang, J.: Heavy air pollution with a unique "non-stagnant" atmospheric boundary layer in the Yangtze River middle basin aggravated by regional transport of PM<sub>2.5</sub> over China, *Atmospheric Chemistry and Physics*, 20, 7217-7230, 10.5194/acp-20-7217-2020, 2020.
- Zhang, J. P., Zhu, T., Zhang, Q. H., Li, C. C., Shu, H. L., Ying, Y., Dai, Z. P., Wang, X., Liu, X. Y., Liang, A. M., Shen, H. X., and Yi, B. Q.: The impact of circulation patterns on regional transport pathways and air quality over Beijing and its surroundings, *Atmospheric Chemistry and Physics*, 12, 5031-5053, 10.5194/acp-12-5031-2012, 2012.

Zhang, Q., Jiang, X., Tong, D., Davis, S. J., Zhao, H., Geng, G., Feng, T., Zheng, B., Lu, Z., Streets, D. G., Ni, R., Brauer, M., van Donkelaar, A., Martin, R. V., Huo, H., Liu, Z., Pan, D., Kan, H., Yan, Y., Lin, J., He, K., and Guan, D.: Transboundary health impacts of transported global air pollution and international trade, *Nature*, 543, 10.1038/nature21712, 2017.

Zhang, Q., Zheng, Y., Tong, D., Shao, M., Wang, S., Zhang, Y., Xu, X., Wang, J., He, H., Liu, W., Ding, Y., Lei, Y., Li, J., Wang, Z., Zhang, X., Wang, Y., Cheng, J., Liu, Y., Shi, Q., Yan, L., Geng, G., Hong, C., Li, M., Liu, F., Zheng, B., Cao, J., Ding, A., Gao, J., Fu, Q., Huo, J., Liu, B., Liu, Z., Yang, F., He, K., and Hao, J.: Drivers of improved PM<sub>2.5</sub> air quality in China from 2013 to 2017, *Proceedings of the National Academy of Sciences of the United States of America*, 116, 24463-24469, 10.1073/pnas.1907956116, 2019.

Zheng, B., Tong, D., Li, M., Liu, F., Hong, C., Geng, G., Li, H., Li, X., Peng, L., Qi, J., Yan, L., Zhang, Y., Zhao, H., Zheng, Y., He, K., and Zhang, Q.: Trends in China's anthropogenic emissions since 2010 as the consequence of clean air actions, *Atmospheric Chemistry and Physics*, 18, 14095-14111, 10.5194/acp-18-14095-2018, 2018.

Zheng, H., Kong, S., Wu, F., Cheng, Y., Niu, Z., Zheng, S., Yang, G., Yao, L., Yan, Q., Wu, J., Zheng, M., Chen, N., Xu, K., Yan, Y., Liu, D., Zhao, D., Zhao, T., Bai, Y., Li, S., and Qi, S.: Intra-regional transport of black carbon between the south edge of the North China Plain and central China during winter haze episodes, *Atmospheric Chemistry and Physics*, 19, 4499-4516, 10.5194/acp-19-4499-2019, 2019a.

Zheng, M., Wang, Y., Bao, J., Yuan, L., Zheng, H., Yan, Y., Liu, D., Xie, M., and Kong, S.: Initial Cost Barrier of Ammonia Control in Central China, *Geophysical Research Letters*, 46, 14175-14184, 10.1029/2019gl084351, 2019b.

Zheng, X. Y., Fu, Y. F., Yang, Y. J., and Liu, G. S.: Impact of atmospheric circulations on aerosol distributions in autumn over eastern China: observational evidence, *Atmospheric Chemistry and Physics*, 15, 12115-12138, 10.5194/acp-15-12115-2015, 2015.

Zhong, J., Zhang, X., Dong, Y., Wang, Y., Liu, C., Wang, J., Zhang, Y., and Che, H.: Feedback effects of boundary-layer meteorological factors on cumulative explosive growth of PM<sub>2.5</sub> during winter heavy pollution episodes in Beijing from 2013 to 2016, *Atmospheric Chemistry and Physics*, 18, 247-258, 10.5194/acp-18-247-2018, 2018.

Bai, Z., Winiwarter, W., Klimont, Z., Velthof, G., Misselbrook, T., Zhao, Z., Jin, X., Oenema, O., Hu, C., and Ma, L.: Further Improvement of Air Quality in China Needs

833 Clear Ammonia Mitigation Target, *Environmental Science & Technology*, 53,  
834 10542-10544, 10.1021/acs.est.9b04725, 2019.

835 Xu, Z., Liu, M., Zhang, M., Song, Y., Wang, S., Zhang, L., Xu, T., Wang, T., Yan, C.,  
836 Zhou, T., Sun, Y., Pan, Y., Hu, M., Zheng, M., and Zhu, T.: High efficiency of  
837 livestock ammonia emission controls in alleviating particulate nitrate during a severe  
838 winter haze episode in northern China, *Atmospheric Chemistry and Physics*, 19,  
839 5605-5613, 10.5194/acp-19-5605-2019, 2019.

840 Ye, Z., Guo, X., Cheng, L., Cheng, S., Chen, D., Wang, W., and Liu, B.: Reducing  
841 PM<sub>2.5</sub> and secondary inorganic aerosols by agricultural ammonia emission  
842 mitigation within the Beijing-Tianjin-Hebei region, China, *Atmospheric*  
843 *Environment*, 219, 10.1016/j.atmosenv.2019.116989, 2019.

844 Cao, J.-J., Shen, Z.-X., Chow, J. C., Watson, J. G., Lee, S.-C., Tie, X.-X., Ho, K.-F.,  
845 Wang, G.-H., and Han, Y.-M.: Winter and Summer PM<sub>2.5</sub> Chemical Compositions  
846 in Fourteen Chinese Cities, *Journal of the Air & Waste Management Association*, 62,  
847 1214-1226, 10.1080/10962247.2012.701193, 2012.

848 Huang, W., Cao, J., Tao, Y., Dai, L., Lu, S.-E., Hou, B., Wang, Z., and Zhu, T.:  
849 Seasonal Variation of Chemical Species Associated With Short-Term Mortality  
850 Effects of PM<sub>2.5</sub> in Xi'an, a Central City in China, *American Journal of*  
851 *Epidemiology*, 175, 556-566, 10.1093/aje/kwr342, 2012.

852 Liu, Z., Gao, W., Yu, Y., Hu, B., Xin, J., Sun, Y., Wang, L., Wang, G., Bi, X., Zhang,  
853 G., Xu, H., Cong, Z., He, J., Xu, J., and Wang, Y.: Characteristics of PM<sub>2.5</sub> mass  
854 concentrations and chemical species in urban and background areas of China:  
855 emerging results from the CARE-China network, *Atmospheric Chemistry and*  
856 *Physics*, 18, 8849-8871, 10.5194/acp-18-8849-2018, 2018.

857 Luo, Y., Zhou, X., Zhang, J., Xiao, Y., Wang, Z., Zhou, Y., and Wang, W.: PM<sub>2.5</sub>  
858 pollution in a petrochemical industry city of northern China: Seasonal variation and  
859 source apportionment, *Atmospheric Research*, 212, 285-295,  
860 10.1016/j.atmosres.2018.05.029, 2018.

861 Wang, H. L., Qiao, L. P., Lou, S. R., Zhou, M., Ding, A. J., Huang, H. Y., Chen, J. M.,  
862 Wang, Q., Tao, S., Chen, C. H., Li, L., and Huang, C.: Chemical composition of  
863 PM<sub>2.5</sub> and meteorological impact among three years in urban Shanghai, China,  
864 *Journal of Cleaner Production*, 112, 1302-1311, 10.1016/j.jclepro.2015.04.099,  
865 2016a.

866 Wang, J., Li, X., Zhang, W., Jiang, N., Zhang, R., and Tang, X.: Secondary PM<sub>2.5</sub> in  
867 Zhengzhou, China: Chemical Species Based on Three Years of Observations,  
868 *Aerosol and Air Quality Research*, 16, 91-104, 10.4209/aaqr.2015.01.0007, 2016b.

- Wang, Q., Fang, J., Shi, W., and Dong, X.: Distribution characteristics and policy-related improvements of PM<sub>2.5</sub> and its components in six Chinese cities, *Environmental Pollution*, 266, 10.1016/j.envpol.2020.115299, 2020.
- Xu, Q., Wang, S., Jiang, J., Bhattarai, N., Li, X., Chang, X., Qiu, X., Zheng, M., Hua, Y., and Hao, J.: Nitrate dominates the chemical composition of PM<sub>2.5</sub> during haze event in Beijing, China, *Science of the Total Environment*, 689, 1293-1303, 10.1016/j.scitotenv.2019.06.294, 2019.
- Zhang, T., Cao, J. J., Tie, X. X., Shen, Z. X., Liu, S. X., Ding, H., Han, Y. M., Wang, G. H., Ho, K. F., Qiang, J., and Li, W. T.: Water-soluble ions in atmospheric aerosols measured in Xi'an, China: Seasonal variations and sources, *Atmospheric Research*, 102, 110-119, 10.1016/j.atmosres.2011.06.014, 2011.
- Zheng, J., Hu, M., Peng, J., Wu, Z., Kumar, P., Li, M., Wang, Y., and Guo, S.: Spatial distributions and chemical properties of PM<sub>2.5</sub> based on 21 field campaigns at 17 sites in China, *Chemosphere*, 159, 480-487, 10.1016/j.chemosphere.2016.06.032, 2016.
- Chang, W., and Zhan, J.: The association of weather patterns with haze episodes: Recognition by PM<sub>2.5</sub> oriented circulation classification applied in Xiamen, Southeastern China, *Atmospheric Research*, 197, 425-436, 10.1016/j.atmosres.2017.07.024, 2017.
- Dai, H., Zhu, J., Liao, H., Li, J., Liang, M., Yang, Y., and Yue, X.: Co-occurrence of ozone and PM<sub>2.5</sub> pollution in the Yangtze River Delta over 2013-2019: Spatiotemporal distribution and meteorological conditions, *Atmospheric Research*, 249, 10.1016/j.atmosres.2020.105363, 2021.
- Ding, A., Huang, X., Nie, W., Chi, X., Xu, Z., Zheng, L., Xu, Z., Xie, Y., Qi, X., Shen, Y., Sun, P., Wang, J., Wang, L., Sun, J., Yang, X.-Q., Qin, W., Zhang, X., Cheng, W., Liu, W., Pan, L., and Fu, C.: Significant reduction of PM<sub>2.5</sub> in eastern China due to regional-scale emission control: evidence from SORPES in 2011-2018, *Atmospheric Chemistry and Physics*, 19, 11791-11801, 10.5194/acp-19-11791-2019, 2019.
- Fu, X., Wang, S., Xing, J., Zhang, X., Wang, T., and Hao, J.: Increasing Ammonia Concentrations Reduce the Effectiveness of Particle Pollution Control Achieved via SO<sub>2</sub> and NO<sub>x</sub> Emissions Reduction in East China, *Environmental Science & Technology Letters*, 4, 221-227, 10.1021/acs.estlett.7b00143, 2017.
- Xing, J., Ding, D., Wang, S., Zhao, B., Jang, C., Wu, W., Zhang, F., Zhu, Y., and Hao, J.: Quantification of the enhanced effectiveness of NO<sub>x</sub> control from simultaneous reductions of VOC and NH<sub>3</sub> for reducing air pollution in the Beijing-Tianjin-Hebei

905 region, China, *Atmospheric Chemistry and Physics*, 18, 7799-7814, 10.5194/acp-18-  
 906 7799-2018, 2018.

907 Xing, J., Ding, D., Wang, S., Dong, Z., Kelly, J. T., Jang, C., Zhu, Y., and Hao, J.:  
 908 Development and application of observable response indicators for design of an  
 909 effective ozone and fine-particle pollution control strategy in China, *Atmospheric*  
 910 *Chemistry and Physics*, 19, 13627-13646, 10.5194/acp-19-13627-2019, 2019.

911 Philipp, A., Beck, C., Huth, R., and Jacobeit, J.: Development and comparison of  
 912 circulation type classifications using the COST 733 dataset and software,  
 913 *International Journal of Climatology*, 36, 2673-2691, 10.1002/joc.3920, 2016.

914 Pope, R. J., Savage, N. H., Chipperfield, M. P., Arnold, S. R., and Osborn, T. J.: The  
 915 influence of synoptic weather regimes on UK air quality: analysis of satellite column  
 916 NO<sub>2</sub>, *Atmospheric Science Letters*, 15, 211-217, 10.1002/asl2.492, 2014.

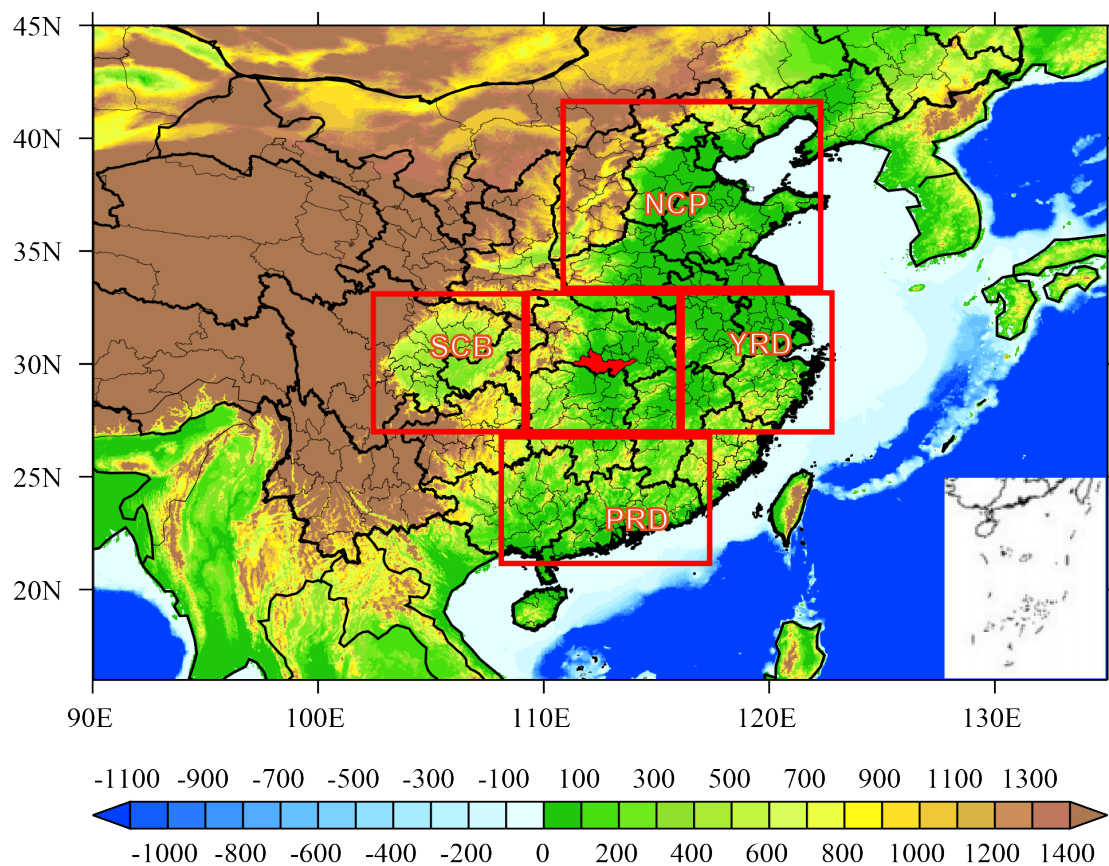
917 Russo, A., Trigo, R. M., Martins, H., and Mendes, M. T.: NO<sub>2</sub>, PM<sub>10</sub> and O<sub>3</sub> urban  
 918 concentrations and its association with circulation weather types in Portugal,  
 919 *Atmospheric Environment*, 89, 768-785, 10.1016/j.atmosenv.2014.02.010, 2014.

920 Santurtun, A., Carlos Gonzalez-Hidalgo, J., Sanchez-Lorenzo, A., and Teresa  
 921 Zarrabeitia, M.: Surface ozone concentration trends and its relationship with weather  
 922 types in Spain (2001-2010), *Atmospheric Environment*, 101, 10-22,  
 923 10.1016/j.atmosenv.2014.11.005, 2015.

924

925

926



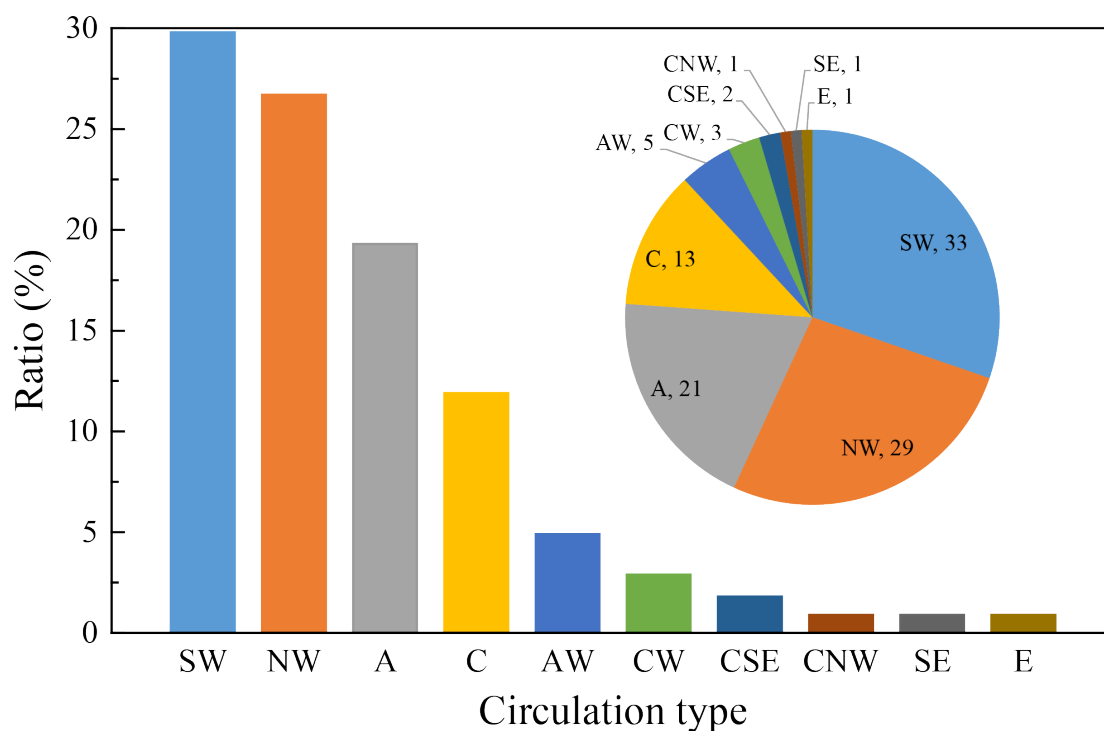
927

928 Figure 1 The location of Jingzhou (red area) and the major haze pollution regions of  
 929 NCP, YRD, PRD, and SCB. The areas framed in red are used to investigate the inter-  
 930 regional impacts by GEOS-Chem sensitivity simulations. The overlaid map shows the  
 931 surface elevation (m) from a 2 min Gridded Global Relief Data (ETOPO2v2) available  
 932 at NGDC Marine Trackline Geophysical database  
 933 (<http://www.ngdc.noaa.gov/mgg/global/etopo2.html>).

934



935

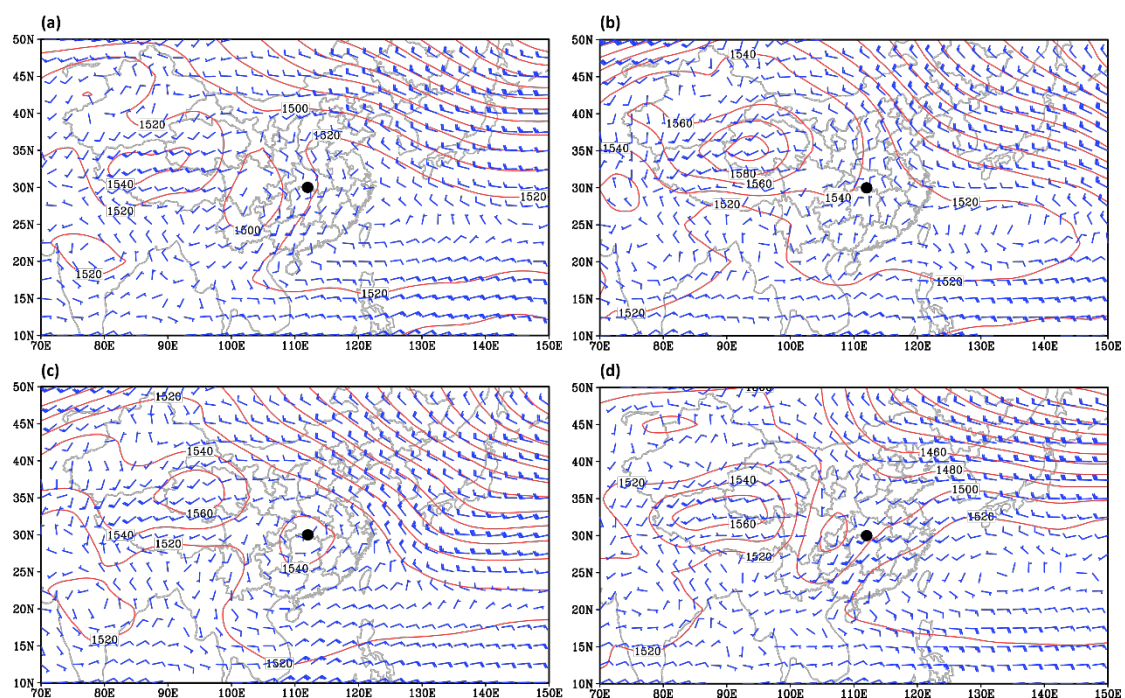


936

937 Figure 2 Frequency distributions of ten circulation types for the heavy pollution days  
 938 of 2013-2018 over Jingzhou. The occurrence numbers of each type are shown. The ten  
 939 circulation types include Southwest (SW), Northwest (NW), Anticyclone (A), Cyclone  
 940 (C), Anticyclone-West (AW), Cyclone-West (CW), Cyclone-Southeast (CSE),  
 941 Cyclone-Northwest (CNW), Southeast (SE) and East (E), respectively.

942

943



944

945 Figure 3 Spatial distribution of 850 hPa geopotential height and wind vector for SW-  
 946 type (a), NW-type (b), A-type (c) and C-type (d) synoptic control averaged over 2013-  
 947 2018. The black dot indicates the location of Jingzhou.

948

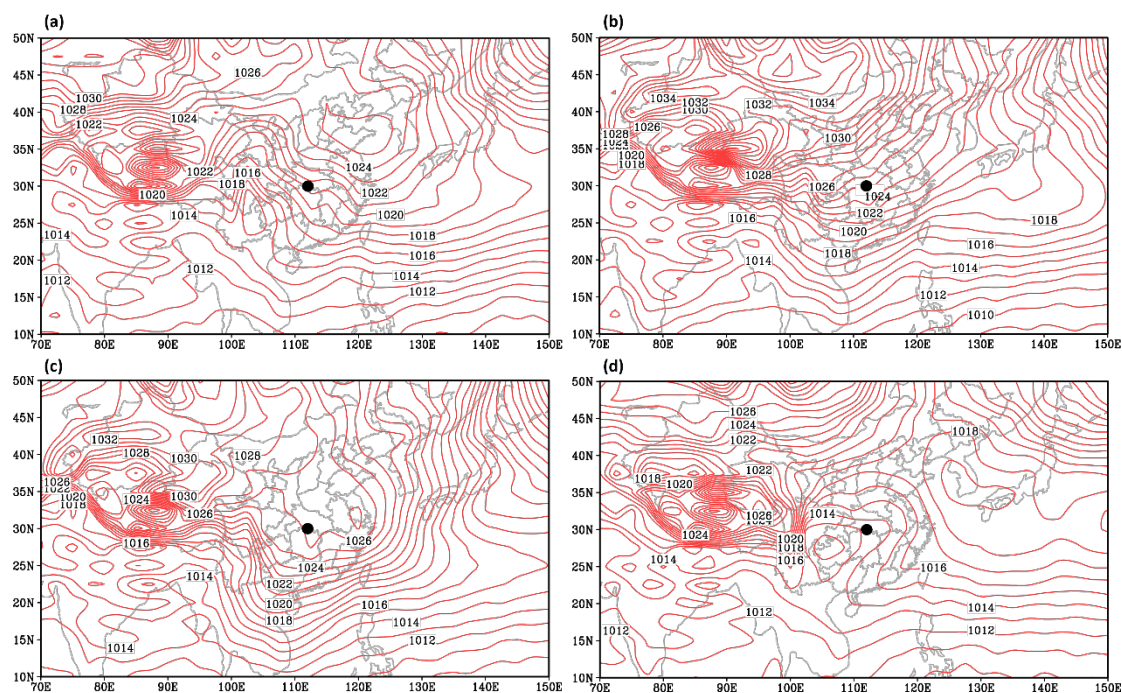
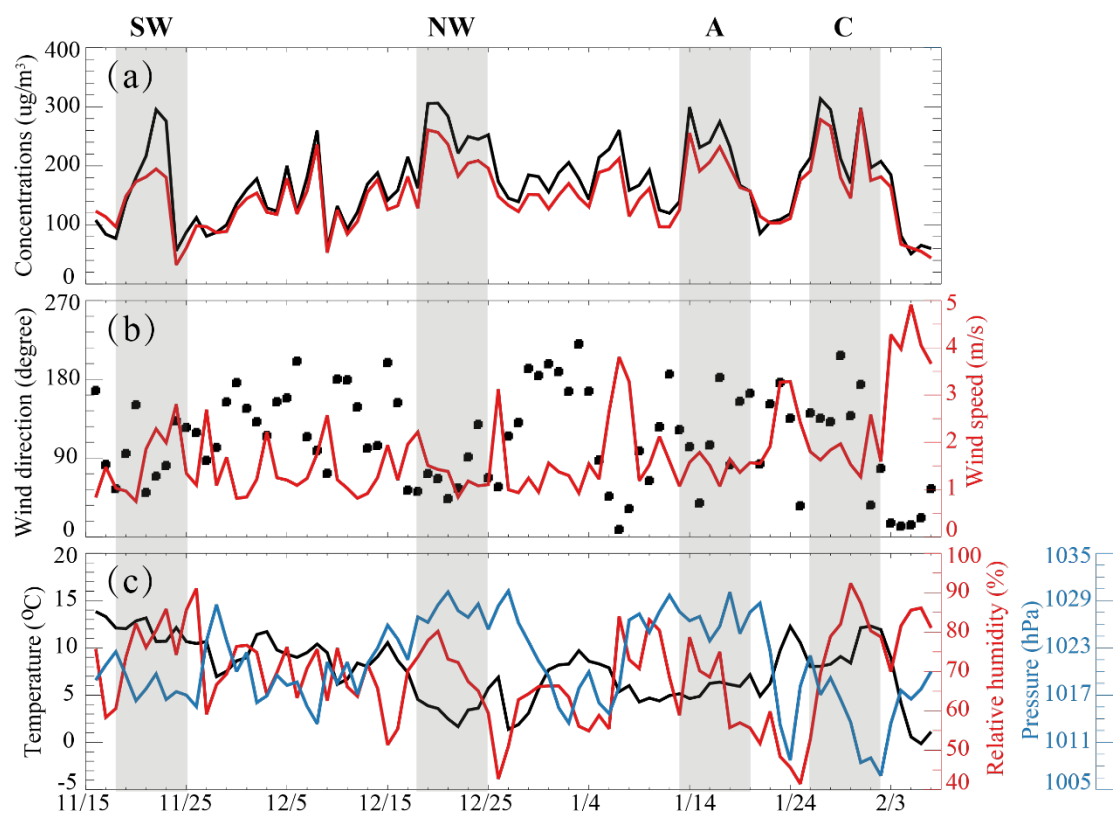


Figure 4 Spatial distribution of sea level pressure for SW-type (a), NW-type (b), A-type (c) and C-type (d) synoptic control averaged over 2013-2018. The black dot indicates the location of Jingzhou.

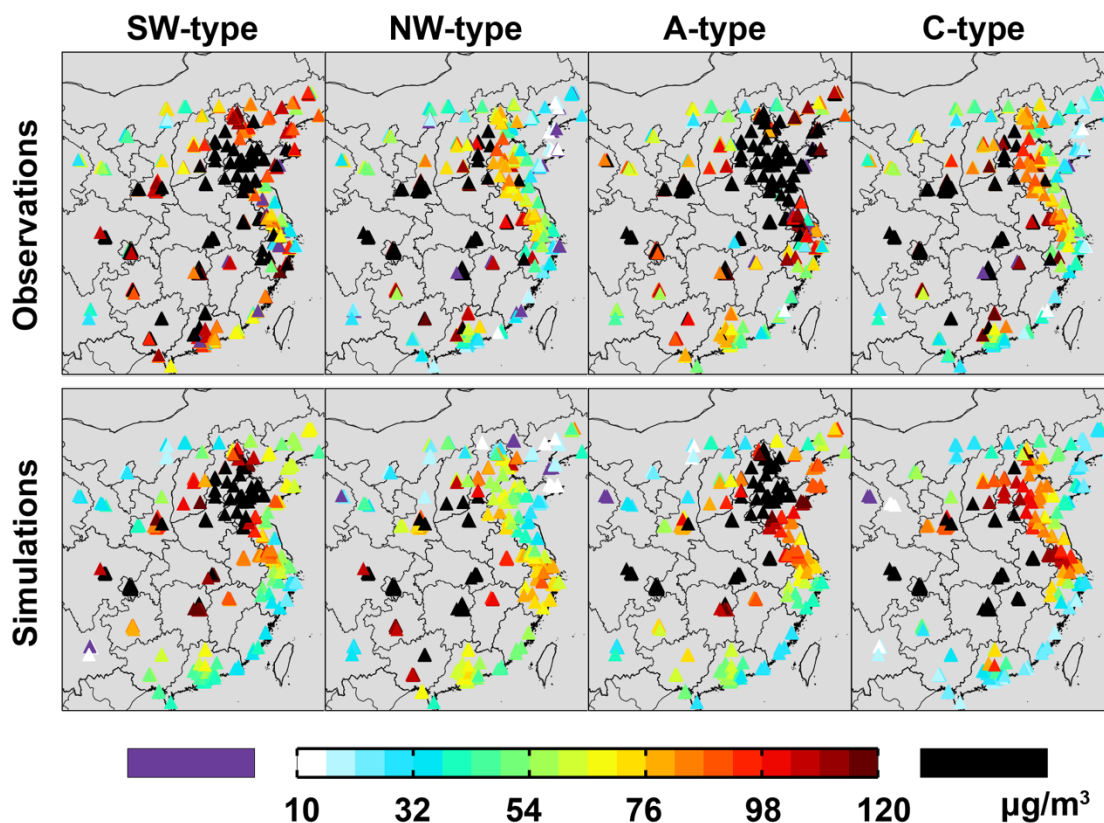


957

958 Figure 5 (a) Daily mean values of modeled (red line) and observed (black line) PM<sub>2.5</sub>  
 959 concentration ( $\mu\text{g}/\text{m}^3$ ) at Jingzhou and four severe pollution events (grey area) from  
 960 November, 2013 to February, 2014. (b) Observed daily mean wind speed (red line) and  
 961 wind direction (black dots). (c) Observed temperature (black line), relative humidity (red  
 962 line) and sea level pressure (blue line).

963

964



966

967 Figure 6 Spatial distribution of observed (top row) and modeled (bottom row, by CON  
 968 case) PM<sub>2.5</sub> concentrations (µg/m<sup>3</sup>) averaged over four severe pollution episodes  
 969 controlled by SW-type (first column), NW-type (second column), A-type (third  
 970 column) and C-type (fourth column) synoptic pattern, respectively.

971

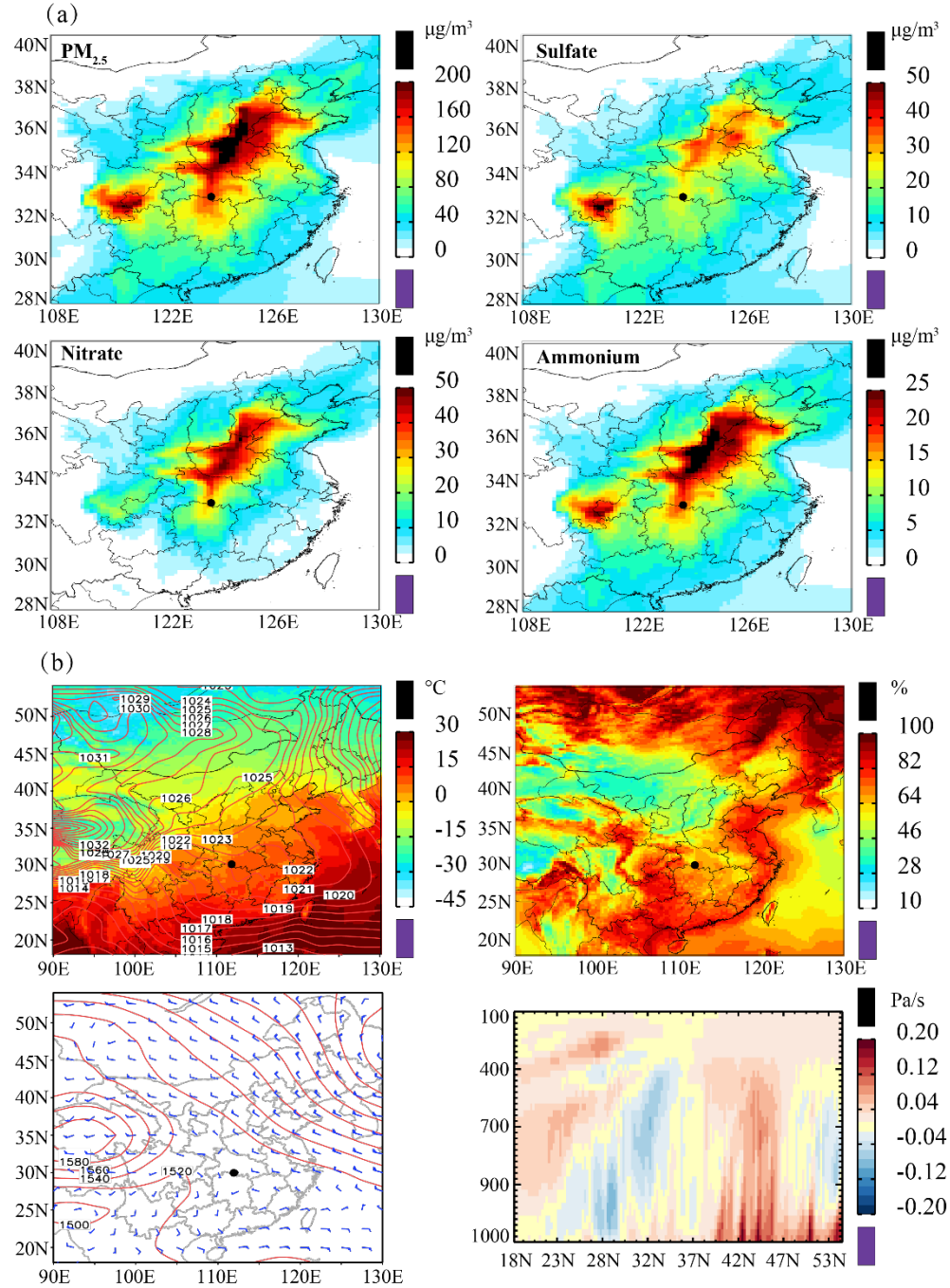
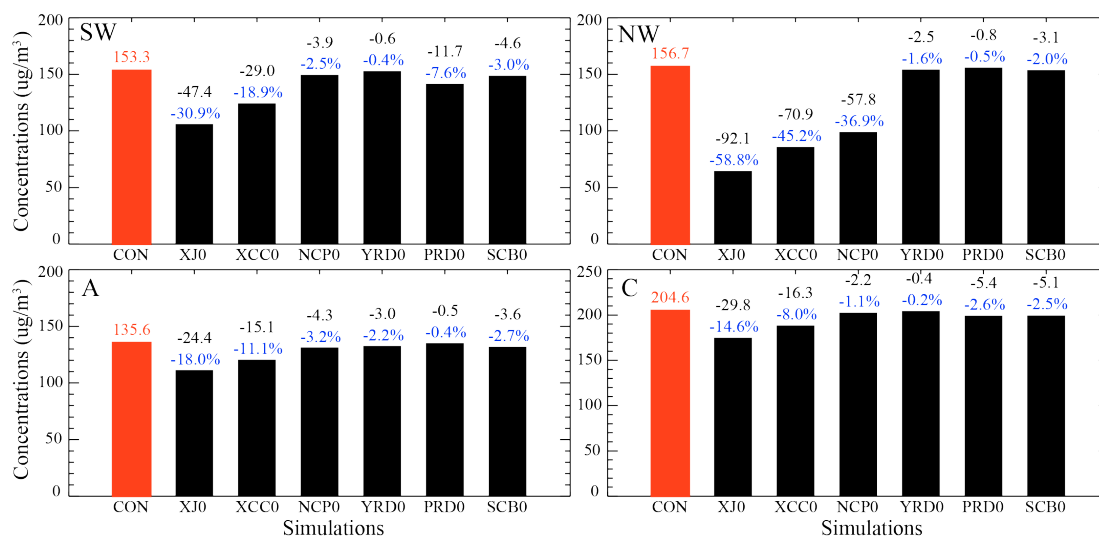


Figure 7 (a) Spatial distribution of  $PM_{2.5}$ , sulfate, nitrate and ammonium concentrations averaged over SW-type synoptic controls (18-25 November, 2013) simulated by GEOS-Chem control simulation ( $\mu g/m^3$ ). (b) Meteorological conditions of SW-type: sea level pressure (red line) and temperature (colour shades), surface relative humidity (%) fields, 850 hPa wind and geopotential height (red line) and height-latitude cross-sections of vertical velocity (Pa/s).



980



981

982 Figure 8 Modeled concentrations ( $\mu\text{g}/\text{m}^3$ ) of  $\text{PM}_{2.5}$  at Jingzhou in the GEOS-Chem  
 983 control (red bar) and sensitivity (black bar) simulations in view of the regional  
 984 transportation, and the differences (black characters for mass concentrations and blue  
 985 characters for mass percentages) between the sensitivity and the control simulations.  
 986 The abbreviations of each simulation referred to Table 2.

987

988

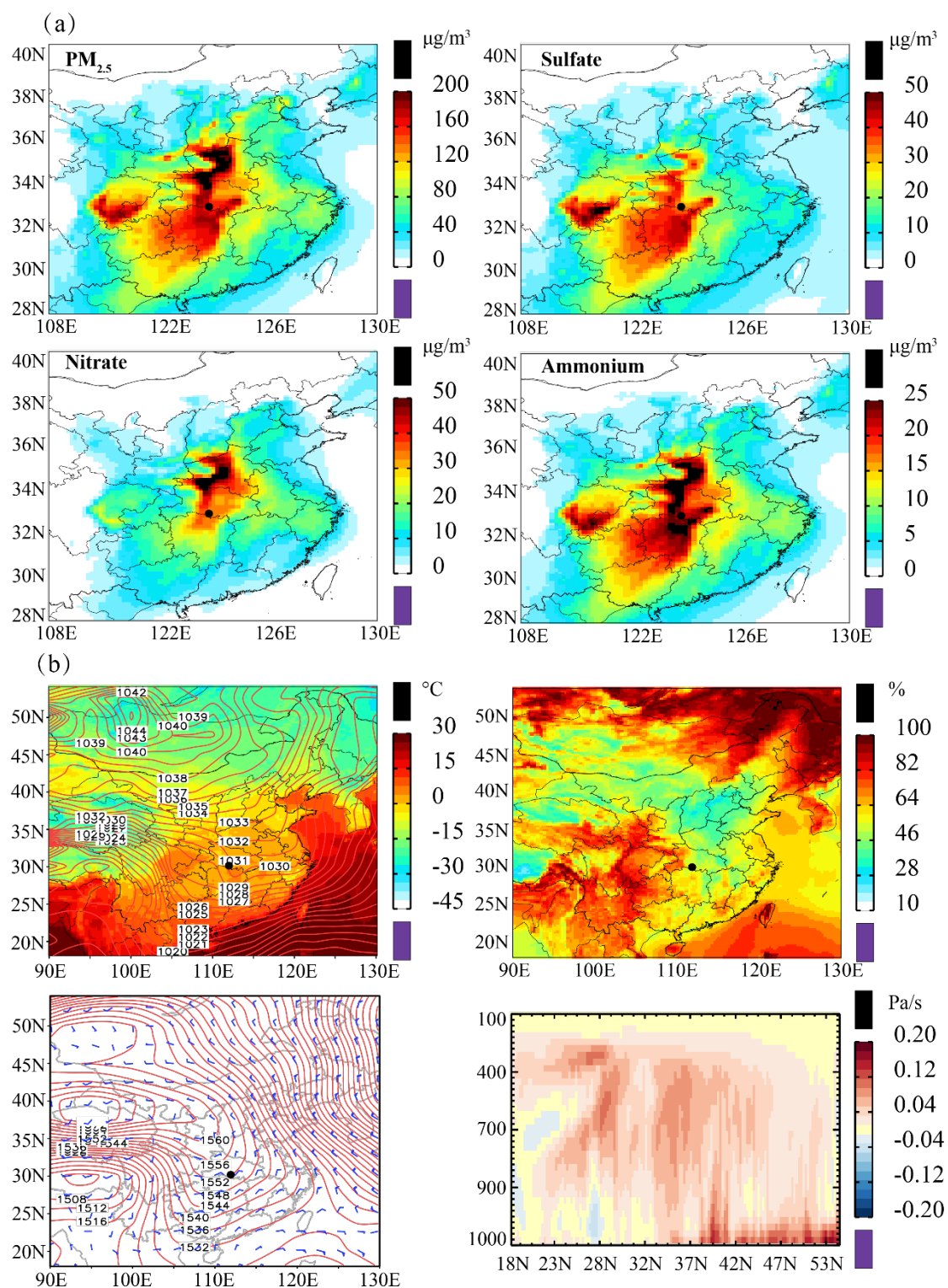


Figure 9 As in Fig. 6 but for NW-type synoptic control (19-26 December, 2013).



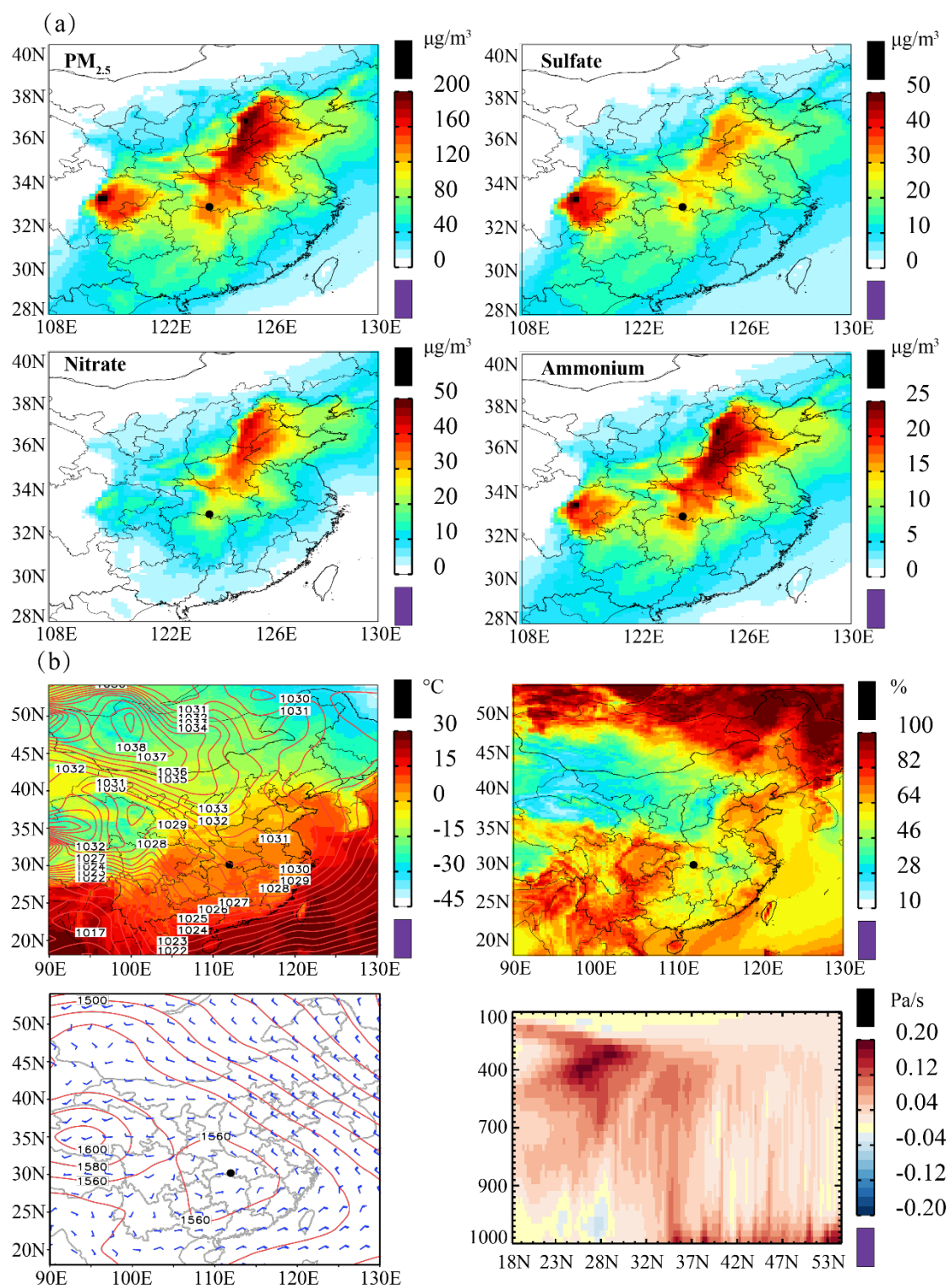


Figure 10 As in Fig. 6 but for A-type synoptic control (14-21 January, 2014).

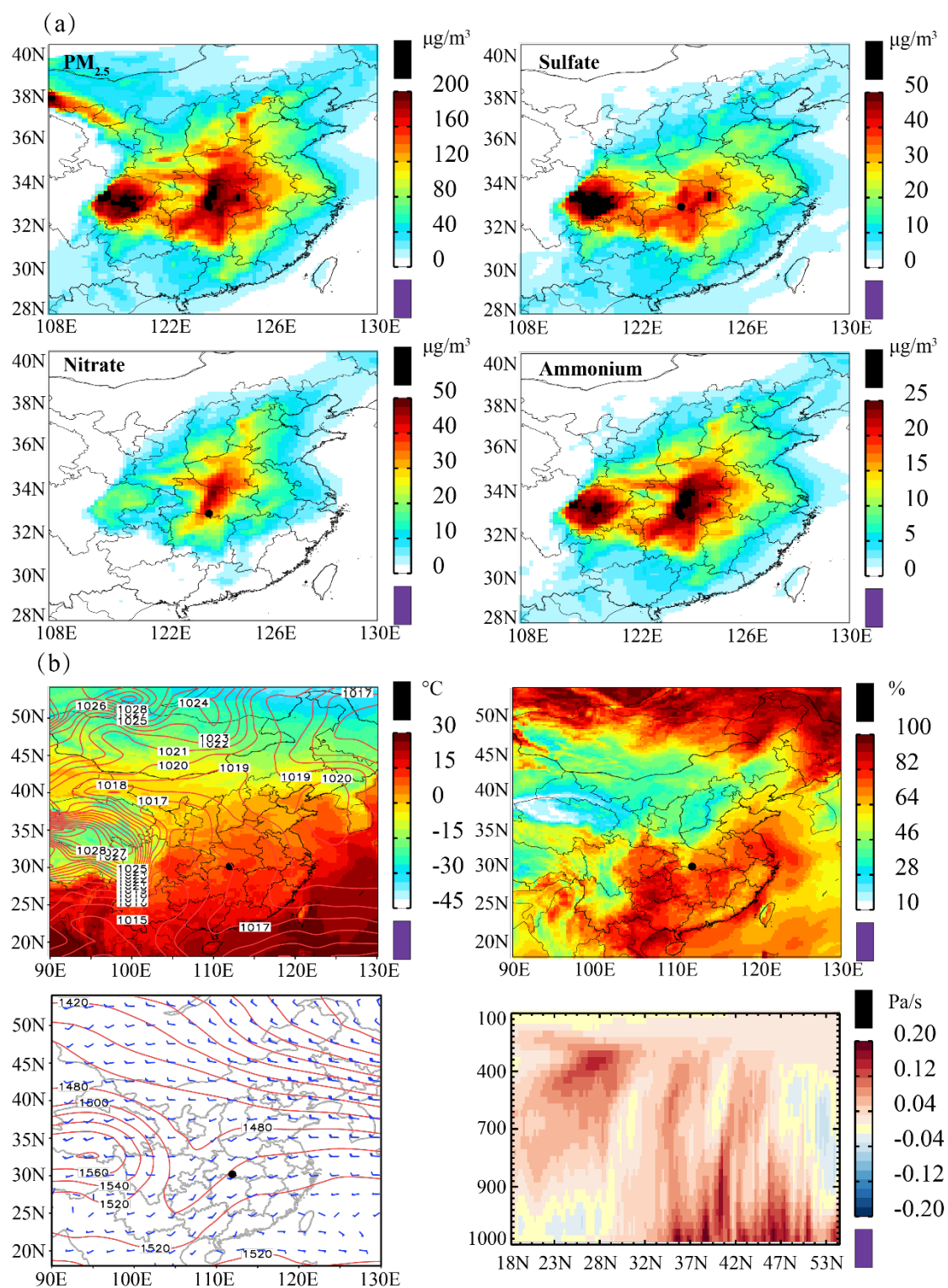
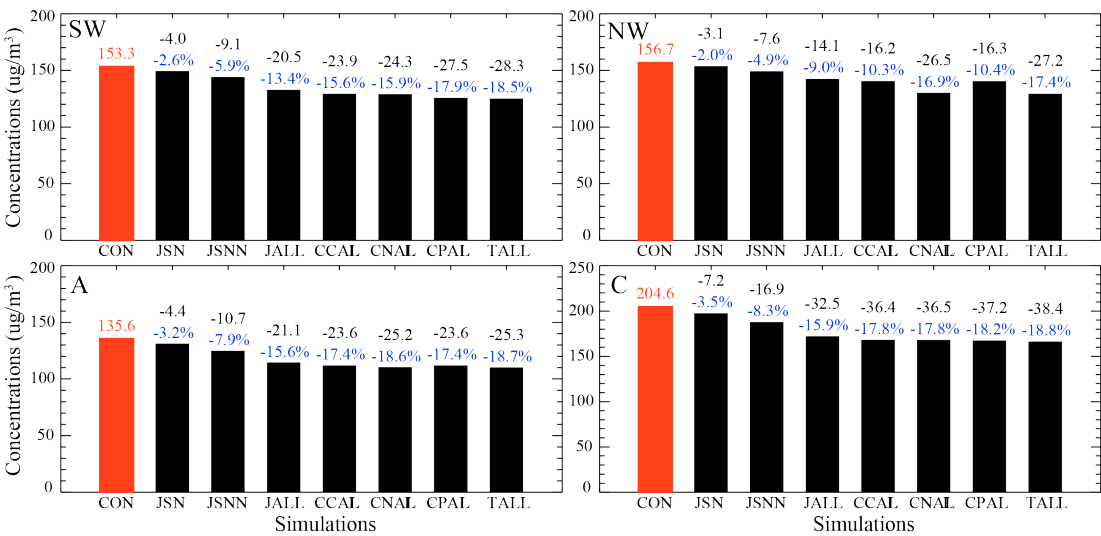


Figure 11 As in Fig. 6 but for C-type synoptic control (26 January - 2 February, 2014).

1004



1005

1006 Figure 12 Modeled concentrations ( $\mu\text{g}/\text{m}^3$ ) of  $\text{PM}_{2.5}$  at Jingzhou in the GEOS-Chem  
1007 control (red bar) and sensitivity (black bar) simulations for emission reduction, and the  
1008 differences (black characters for mass concentrations and blue characters for mass  
1009 percentages) between the sensitivity and the control simulations. The abbreviations of  
1010 each simulation referred to Table 2.

1011

1012

1013

1014 Table 1 Lamb-Jenkinson circulation types

$ \xi  \leq V$	$ \xi  \geq 2V$	$V <  \xi  < 2V$
(Flat airflow type)	(Rotating airflow type)	(Mixed type)
East (E), Southeast (SE), Southwest (SW), Northwest (NW)	Anticyclone (A), Cyclone (C)	Cyclone-Southeast (CSE), Cyclone-West (CW), Cyclone-Northwest (CNW), Anticyclone-West (AW)

1015

1016

1017

1018 Table 2 Description of sensitivity simulations by GEOS-Chem model. The NCP, YRD,  
 1019 PRD and SCB are the areas framed in red showed by Fig. 1.

Simulations	Description
CON	Applying the original emission situation in Table S1 and Table S2
XJ0	Emissions of all pollution sources <sup>1</sup> outside Jingzhou are set to be zero
XCC0	Emissions of all pollution sources outside Central China are set to be zero
NCP0	Emissions of all pollution sources over NCP region are set to be zero
YRD0	Emissions of all pollution sources over YRD region are set to be zero
PRD0	Emissions of all pollution sources over PRD region are set to be zero
SCB0	Emissions of all pollution sources over SCB region are set to be zero
JSN	Emissions of SO <sub>2</sub> and NO <sub>x</sub> at Jingzhou are reduced by 20%
JSNN	Emissions of SO <sub>2</sub> , NO <sub>x</sub> and NH <sub>3</sub> at Jingzhou are reduced by 20%
JALL	Emissions of all pollution sources at Jingzhou are reduced by 20%
CCALL	Emissions of all pollution sources over Central China are reduced by 20%
CNALL	Emissions of all pollution sources over Central China and NCP region are reduced by 20%
CPALL	Emissions of all pollution sources over Central China and PRD region are reduced by 20%
TALL	Emissions of all pollution sources over Central China, NCP, YRD, PRD and SCB region are reduced by 20%

1020 1. All pollution sources include emissions of SO<sub>2</sub>, NO<sub>x</sub>, NH<sub>3</sub>, CO, BC, OC and NMVOCs.

1021

1022

1023

1024

1025 Table 3 Simulated PM<sub>2.5</sub> concentrations and associated chemical components averaged  
 1026 for the four typical heavy pollution episodes at Jingzhou. Also shown in brackets are  
 1027 the percentages of each component in PM<sub>2.5</sub>.

PM <sub>2.5</sub> components	Typical heavy pollution episodes			
μg/m <sup>3</sup>	11/18-11/25 (SW-type)	12/19-12/26 (NW-type)	1/14-1/21 (A-type)	1/26-2/2 (C-type)
Nitrate	30.6 (20.0%)	34.6 (22.1%)	23.4 (17.3%)	42.3 (20.7%)
Sulfate	26.5 (13.4%)	30.7 (19.6%)	27.7 (20.4%)	40.4 (19.7%)
Ammonium	18.8 (12.3%)	21.6 (13.8%)	17.1 (12.6%)	27.1 (13.2%)
Dust	24.4 (15.9%)	22.3 (14.2%)	19.8 (14.6%)	29.2 (14.3%)
BC	10.5 (6.8%)	9.6 (6.1%)	9.5 (7.0%)	13.8 (6.7%)
POA	21.6 (14.1%)	18.9 (12.1%)	18.9 (13.9%)	27.7 (13.5%)
SOA	20.9 (13.6%)	19.0 (12.1%)	19.2 (14.2%)	24.1 (11.8%)
PM <sub>2.5</sub>	153.3	156.7	135.6	204.6

1028

1029

1030 Table 4 The reported concentrations of PM<sub>2.5</sub> and the three inorganic salts (sulfate,  
1031 nitrate and ammonium, µg/m<sup>3</sup>) in other cities.

References	Site	Time	PM <sub>2.5</sub>	Sulfate	Nitrate	Ammonium
Cao et al., 2012	Beijing	01/03	115.6±46.6	20.0±4.2 (17.3%)	13.1±4.5 (11.3%)	9.4±4.1 (8.1%)
Cao et al., 2012	Qingdao	01/03	134.8±43.0	21.1±7.7 (15.7%)	19.3±9.2 (14.3%)	15.3±5.2 (11.4%)
Cao et al., 2012	Tianjin	01/03	203.1±76.2	32.5±15.1 (16.0%)	25.2±10.3 (12.4%)	22.2±9.8 (10.9%)
Cao et al., 2012	Xi'an	01/03	356.3±118.4	53.8±25.6 (15.1%)	29.0±10.0 (8.1%)	29.8±11.5 (8.4%)
Cao et al., 2012	Chongqing	01/03	316.6±101.2	60.9±19.6 (19.2%)	18.1±6.4 (5.7%)	28.8±8.9 (9.1%)
Cao et al., 2012	Hangzhou	01/03	177.3±59.5	33.4±16.7 (18.8%)	25.7±14.8 (14.5%)	19.1±10.7 (10.8%)
Cao et al., 2012	Shanghai	01/03	139.4±50.6	21.6±12.3 (15.5%)	17.5±8.7 (12.6%)	14.5±5.9 (10.4%)
Cao et al., 2012	Wuhan	01/03	172.3±67.0	31.4±15.6 (18.2%)	22.2±10.7 (12.9%)	18.4±10.2 (10.7%)
Zhang et al., 2011	Xi'an	03/06-03/07	194.1	35.6 (18.3%)	16.4 (8.4%)	11.4 (5.9%)
Huang et al., 2012	Xi'an	01/06-02/06	235.8±125.1	44.8±31.3 (19.0%)	20.5±14.2 (8.7%)	14.5±10.8 (6.1%)
Wang et al., 2020	Jinan	10/17	104±54	14.4±9.2 (13.8%)	33.4±23.2 (32.1%)	13.0±8.3 (12.5%)
Wang et al., 2020	Shijiazhuang	10/17	152±109	19.3±19.6 (12.7%)	42.8±41.1 (28.2%)	18.2±17.1 (12.0%)
Wang et al., 2020	Wuhan	12/17	117±33	13.6±3.2	26.6±11.1	13.1±3.8

				(11.6%)	(22.7%)	(11.2%)
Wang et al., 2016a	Zhengzhou	01/11-02/11	297±160	48±36 (16.2%)	31±19 (10.4%)	21±16 (7.1%)
Wang et al., 2016a	Zhengzhou	01/12-02/12	234±125	23±10 (9.8%)	22±9 (9.4%)	16±5 (6.8%)
Wang et al., 2016a	Zhengzhou	01/13-02/13	337±168	56±39 (16.6%)	39±20 (11.6%)	31±18 (9.2%)
Luo et al., 2018	Zibo	12/06-02/07	224.9±85.4	40.1±19.2 (17.9%)	18.1±9.0 (8.1%)	21.7±10.2 (9.7%)
Wang et al., 2016b	Shanghai	12/11, 12/12, 12/13	73.9±57.5	12.2±9.2 (16.5%)	14.6±12.2 (19.8%)	8.2±6.7 (11.1%)
Xu et al., 2019	Beijing	02/17-03/17	180.5	20.1 (11.1%)	45.6 (25.3%)	22.5 (12.5%)
Xu et al., 2019	Beijing	05/17-09/17	186.7	20.2 (10.8%)	32.4 (17.4%)	17.1 (9.2%)
Xu et al., 2019	Beijing	10/17-11/17	167.5	17.9 (10.7%)	44.5 (26.6%)	20.9 (12.5%)
Zheng et al., 2016	Beijing	03/10-05/10	65.2±65.1	11.1±10.1 (17.0%)	11.1±11.0 (17.0%)	6.8±6.7 (10.4%)
Zheng et al., 2016	Beijing	07/09-08/09	88.9±39.1	23.0±13.9 (25.9%)	16.2±11.8 (18.2%)	11.8±6.8 (13.3%)
Zheng et al., 2016	Beijing	12/09-02/10	84.0±66.6	8.1±8.3 (9.1%)	8.0±9.6 (9.0%)	5.9±7.1 (6.6%)
Zheng et al., 2016	Guangzhou	11/10	73.3±16.5	16.6±4.0 (22.6%)	5.7±3.8 (7.8%)	6.2±2.0 (8.5%)
Zheng et al., 2016	Shenzhen	12/09	64.6±24.7	20.6±3.5 (31.9%)	4.9±3.5 (7.6%)	4.6±1.0 (7.1%)
Zheng et al., 2016	Wuxi	04/10-05/10	82.1±27.0	12.8±3.8	9.9±6.3	7.0±2.0



				(15.6%)	(12.1%)	(8.5%)
Zheng et al., 2016	Jinhua	10/11-11/11	81.9±26.2	18.3±6.7 (22.3%)	12.6±7.0 (15.4%)	10.4±4.1 (12.7%)
Liu et al., 2018	Chongqing	2012-2013	73.5±30.5	19.7±9.6 (26.8%)	6.5±6.2 (8.8%)	6.1±2.7 (8.3%)
Liu et al., 2018	Shanghai	2012-2013	68.4±20.3	13.6±6.4 (19.9%)	11.9±5.0 (17.4%)	5.8±2.1 (8.5%)
Liu et al., 2018	Beijing	2012-2013	71.7±36.0	11.9±8.2 (16.6%)	9.3±7.5 (13.0%)	5.3±2.7 (7.4%)

1032